PROTEINS: Structure, Function, and Bioinformatics 68:458–479 (2007)

Multiple Asparagine Deamidation of *Bacillus anthracis* Protective Antigen Causes Charge Isoforms Whose Complexity Correlates With Reduced Biological Activity

Bradford S. Powell,* Jeffrey T. Enama, Wilson J. Ribot, Wendy Webster, Stephen Little, Timothy Hoover, Jeffrey J. Adamovicz, and Gerard P. Andrews

Bacteriology Division, United States Army Medical Research Institute of Infectious Diseases, Fort Detrick, Frederick, Maryland 21702-5011

ABSTRACT **Protective antigen is essential for the pathology of *Bacillus anthracis* and is the proposed immunogen for an improved human anthrax vaccine. Known since discovery to comprise differentially charged isoforms, the cause of heterogeneity has eluded specific structural definition until now. Recombinant protective antigen (rPA) contains similar isoforms that appear early in fermentation and are mostly removed through purification. By liquid chromatography-tandem mass spectrometry sequencing of the entire protein and inspection of spectral data for amino acid modifications, pharmaceutical rPA contained measurable deamidation at seven of its 68 asparagine residues. A direct association between isoform complexity and percent deamidation was observed such that each decreased with purity and increased with protein aging. Position N537 consistently showed the highest level of modification, although its predicted rate of deamidation ranked 10th by theoretical calculation, and other asparagines of higher predicted rates were observed to be unmodified. rPA with more isoforms and greater deamidation displayed lower activities for furin cleavage, heptamerization, and holotoxin formation. Lethal factor-mediated macrophage toxicity correlated inversely with deamidation at residues N466 and N408. The described method measures deamidation without employing theoretical isotopic distributions, comparison between differentially treated samples or computational predictions of reactivity rates, and is broadly applicable to the characterization of other deamidated proteins. Proteins 2007;68:458–479.** © 2007 Wiley-Liss, Inc.

Key words: anthrax vaccine; anthrax toxin; protein degradation; iso-aspartate; succinimide intermediate; heavy isotope; two-dimensional gel electrophoresis; capillary isoelectric focusing; computational model; liquid chromatography-ion trap tandem mass spectrometry

INTRODUCTION

The protective antigen (PA) of *Bacillus anthracis* plays an essential role in anthrax pathology, and is under investigation as the proposed key component for a new human anthrax vaccine to protect against the aerosol route of infection.[1–3] Functioning as a bipartite exotoxin during disease,[4] PA is the receptor-binding and cytoplas-

Abbreviations: 2-DE, two-dimensional polyacrylamide gel electrophoresis; ATR, anthrax toxin receptor; AVA, anthrax vaccine adsorbed; CIEF, capillary isoelectric focusing; Da, Dalton; EC_{50}, 50% effective concentration; EF, edema factor; EIC, extracted ion chromatogram; ESI, electrospray ionization; FDA, Food and Drug Administration; GMP, good manufacturing practices; HEPES, (4-(2-hydroxyethyl)-1-piperazineethanesulfonic acid; ICC, ion charge control; isoAsp, isoaspartate; LC/MSD, liquid chromatograph/mass selective detector; LC-MS/MS, liquid chromatography trap tandem mass spectrometry (performed only with electrospray ionization source and ion trap analysis in this article); LF, lethal factor; m/z, mass to charge ratio; MALDI-TOF-MS, matrix assisted laser desorption ionization time of flight mass spectrometry; M_r, relative molecular mass; MTT, 2,5-diphenyltetrazolium bromide; PA, *B. anthracis* protective antigen; PBS, phosphate-buffered saline; PIMT, protein L-isoaspartyl *O*-methyltransferase; R_m, relative mobility; rPA, recombinant protective antigen; RP-HPLC, reversed phase high-pressure liquid chromatography; SDS-PAGE, sodium dodecyl sulfate polyacrylamide gel electrophoresis; SPI, Scored peak intensity is the percentage of the spectral peak-detected ion current prescribed by the automated search interpretation criteria; SPS, smart parameter settings; T_a, anode interface; T_c, cathode interface; TIC, total ion chromatogram; T_p, analyte migration time; USAMRIID, United States Medical Research Institute of Infectious Diseases.

Opinions, interpretations, conclusions, and recommendations are those of the authors and are not necessarily endorsed by the U.S. Army.

Preliminary portions of this work were publicly released at the following venues: Mass Spectrometry Interest Group Seminar Series, National Cancer Institute, June 8, 2004; The Greenbaum Cancer Center Proteomics Interest Group, November 19, 2004; 24th Army Science Conference, Nov 29–Dec 2, 2004; The Pittsburg Conferences on Analytical Chemistry and Applied Spectroscopy, Feb 28–March 3, 2005 and March 12–17 2006.

Grant sponsor: U.S. Army Medical Research and Materiel Command; Grant number: DAM17-98-D-0029, Project 02-4-CC-010, 02-4-CC-008, and 02-4-5C-023.

Gerard P. Andrews's Current address is Department of Veterinary Sciences, UW, Wyoming State Veterinary Laboratory 1174 Snowy Range Road, Laramie, WY 82070.

*Correspondence to: Bradford S. Powell, Ph.D., Bacteriology Division, United States Army Medical Research Institute of Infectious Diseases, 1425 Porter Street, Fort Detrick, Frederick, MD 21702-5011. E-mail: bradford.powell@det.amedd.army.mil

Received 29 September 2006; Revised 27 December 2006; Accepted 17 January 2007

Published online 27 April 2007 in Wiley InterScience (www.interscience.wiley.com). DOI: 10.1002/prot.21432

Report Documentation Page

Form Approved
OMB No. 0704-0188

1. REPORT DATE	2. REPORT TYPE	3. DATES COVERED
1 FEB 2007	**N/A**	**-**

4. TITLE AND SUBTITLE
Multiple asparagine deamidation of Bacillus anthracis protective antigen causes charge isoforms whose complexity correlates with reduced biological activity. Proteins: Structure, Function, and Bioinformatics 68:458-479

5a. CONTRACT NUMBER

5b. GRANT NUMBER

5c. PROGRAM ELEMENT NUMBER

6. AUTHOR(S)
Powell, BS Enama, JT Ribot, WJ Webster, W Little, S Hoover, T Adamovicz, JJ Andrews, GP

5d. PROJECT NUMBER

5e. TASK NUMBER

5f. WORK UNIT NUMBER

7. PERFORMING ORGANIZATION NAME(S) AND ADDRESS(ES)
United States Army Medical Research Insitute of Infectious Diseases, Fort Detrick, MD

8. PERFORMING ORGANIZATION REPORT NUMBER
TR-06-120

9. SPONSORING/MONITORING AGENCY NAME(S) AND ADDRESS(ES)

10. SPONSOR/MONITOR'S ACRONYM(S)

11. SPONSOR/MONITOR'S REPORT NUMBER(S)

12. DISTRIBUTION/AVAILABILITY STATEMENT
Approved for public release, distribution unlimited

13. SUPPLEMENTARY NOTES

14. ABSTRACT

Protective antigen is essential to the pathology of Bacillus anthracis and is the proposed immunogen for an improved human anthrax vaccine. Known since discovery to comprise differentially charged isoforms, the cause of heterogeneity has eluded specific structural definition until now. Recombinant protective antigen (PA) contains similar isoforms which appear early in fermentation and are mostly removed through purification. By liquid chromatography-tandem mass spectrometry sequencing of the entire protein and inspection of spectral data for amino acid modifications, pharmaceutical grade rPA contained measurable deamidation at 7 of its 68 asparagine residues. A direct association between isoform complexity and percent deamidation was observed such that each decreased with purity and increased with protein aging. Position N537 consistently showed the highest level of modification, although its predicted rate of deamidation ranked 10th by theoretical calculation, and other asparagines of higher predicted rates were observed to be unmodifed. rPA with more isoforms and greater deamidation displayed lower activities for furin cleavage, heptamerization, and holotoxin formation. Lethal factor-mediated macrophage toxicity correlated inversely with rPA deamidation. The described method measures deamidation without comparison to theoretical isotopic distributions, algorithmic predictions of reactivity, or differentially treated samples, and is broadly applicable to the characterization of other deamidated proteins.

15. SUBJECT TERMS
Bacillus anthracis, anthrax, vaccine, protective antigen, PA, isoforms, deamidation,iso-aspartate, heavy isotope, two-dimensional gel electrophoresis, capillary isoelectric focusing, ion trap, liquid chromatography tandem mass spectrometry

16. SECURITY CLASSIFICATION OF:			17. LIMITATION OF ABSTRACT	18. NUMBER OF PAGES	19a. NAME OF RESPONSIBLE PERSON
a. REPORT **unclassified**	b. ABSTRACT **unclassified**	c. THIS PAGE **unclassified**	**UU**	**24**	

Standard Form 298 (Rev. 8-98)
Prescribed by ANSI Std Z39-18

mic transporter component for two catalytic moieties, edema factor (EF), which is a calmodulin-sensitive adenylate cyclase, and lethal factor (LF), a Zn^{2+}-dependent endoproteinase of mitogen-activated protein kinase kinases.[5–8] The deregulation of cellular physiology by EF and LF leads to tissue swelling, necrosis, shock, and rapid death if untreated, all hallmark symptoms of anthrax.[9] PA protein (83 kDa) binds to cell-surface anthrax toxin receptors (ATR)[10] and is cleaved by the furin family of proteases[11] to create a 63 kDa active form and a 20 kDa fragment of undefined function.[12] Cleaved PA_{63} assembles into a heptameric prepore $(PA_{63})_7$ that binds up to three molecules of EF or LF.[13,14] This complex is endocytosed and trafficked to an acidic compartment wherein a large loop from domain 2 in each PA subunit inserts into the membrane and forms a 14-strand β-barrel.[15–18] A model of translocation[19,20] proposes that the EF (89 kDa) and LF (90 kDa) pass through the channel of this pore. This model invokes unfolding of EF and LF for transit, with spontaneous refolding in the target cell's cytosol, since the X-ray structures of EF and LF have minimum measured diameter of ~45 Å, while the PA pore has a diameter of ~12 to ~17 Å.[18] Alternatively, full endoproteinase activity of LF was demonstrated to occur without dissociation from the membrane-bound PA complex.[21] Although the precise mechanism is still uncertain, it is clear that factor binding is essential and the net effect of PA activity is to expose targeted host cells to the catalytic cytotoxic factors. By itself, however, PA is nontoxic and elicits protective immunity against *B. anthracis*, as demonstrated by numerous animal studies.[2,22,23] Because of its pivotal role in pathogenesis and its immunoprotective activity, PA has accordingly been an unknown or intended principal constituent in anthrax vaccines since the first demonstration of protective preparations 125 years ago.[1,22]

The modern search for a safe and effective human anthrax vaccine has led to the development of purified recombinant PA (rPA),[3,23,24] considered the top candidate for the first subunit vaccine to replace existing anthrax vaccines, which are comprised of alum-precipitated *B. anthracis* culture supernatant preserved with formalin. The currently licensed human anthrax vaccines (BioThrax®, BioPort, Lansing MI; and Anthrax Vaccine Precipitated, Porton Down, UK) are based on 50-year-old technology, are reactogenic and require multiple doses to impart full immunity with annual boosting for maintenance.[1–3] In addition, they contain many cellular components besides PA of unspecified influence on product effectiveness and safety.[25] Animal studies have demonstrated that purified rPA elicits equivalent immunogenicity and protective immunity compared with these licensed vaccines.[2,3,26–28] As an active pharmaceutical ingredient intended for eventual use in humans, rPA requires thorough characterization in many aspects of product safety and effectiveness, including detailed descriptions of biological activity and chemical structure. When heterogeneity is evident in a proposed biological product, as is the case for rPA, FDA regulation specifies the documentation of methods and results that provide increased understanding of its physicochemical and molecular structure.[29,30] With regard to biological activity *in vivo*, prior investigation has shown that the two major isoforms and principal components of pharmaceutical grade rPA elicit equivalent specific immunity and protection against lethal challenge by *B. anthracis* spores.[23] The analytical method and findings reported here reveal multiple site deamidation as the chemical source of micro-heterogeneity that was long observed as negatively charged isoforms in native PA protein.

Purified proteins are particularly susceptible to degradation through the nonenzymatic post-translational modifications of deamidation, oxidation, and aggregation.[31,32] Because any of these modifications may affect the composition, quality, consistency, or stability of the final form, degradation activities introduce the need for special controls during the manufacture, storage, and use of purified proteins intended for scientific study or commerce. Deamidation is generally the most prevalent of these spontaneous changes to protein structure.[31–39] The deamidation reaction, which is the loss of ammonia from the amide side group of asparagine (Asn) or glutamine (Gln), proceeds through a cyclic imide intermediate (see Fig. 1) whose rate of formation and hydrolysis is strongly affected by the adjoining distal amino acid, local spatial structure, and solvation chemistry, including pH and solute composition.[33–39] Deamidation introduces an ionizable carboxylate group, which imparts a negative charge at physiological pH and increases the mass of the protein by 1 Da. Asparagine residues were first observed to be ~40 times more prone to deamidation than Gln residues within proteins.[34] More recently, extensive studies of model synthetic peptides indicate that Asn residues deamidated on average about 100 times faster than do Gln residues in peptides.[40] Consequently, most experimental observations concern Asn deamidation and commonly measure one of its two reaction products. Although, Asn deamidation yields normal L-aspartate (Asp), the more abundant product is isoaspartate (isoAsp), a β-linked isomer which incorporates the side chain C_β into the peptide backbone (see Fig. 1).[34] Because isoAsp also lengthens the polypeptide chain by one methylene group (CH_2), it is more deleterious to protein structure and function,[32,35,39,41] and consequently has attracted more attention in the characterization of protein stability.[31,42,43] This aberrant β-isopeptidyl bond is corrected *in vivo* by protein L-isoaspartyl *O*-methyltransferase (PIMT, EC2.1.1.77), an enzyme first discovered in brain tissue, but which now appears to be widely distributed and critical for alleviating this form of protein aging.[36,41,44] A growing list of maladies and cellular dysfunctions are associated with PIMT deficiency, increased isoAsp content, or Asn/Gln deamidation, including cataracts,[45,46] Alzheimer's disease,[47,48] spina bifida,[49] autoimmunity,[50] and prion-related encephalopathies.[51,52] Spontaneous deamidation has also been associated with normal processes, such as Bcl-x_L-regulated apoptosis[53] and homeostasis of cytochrome C.[54] Because

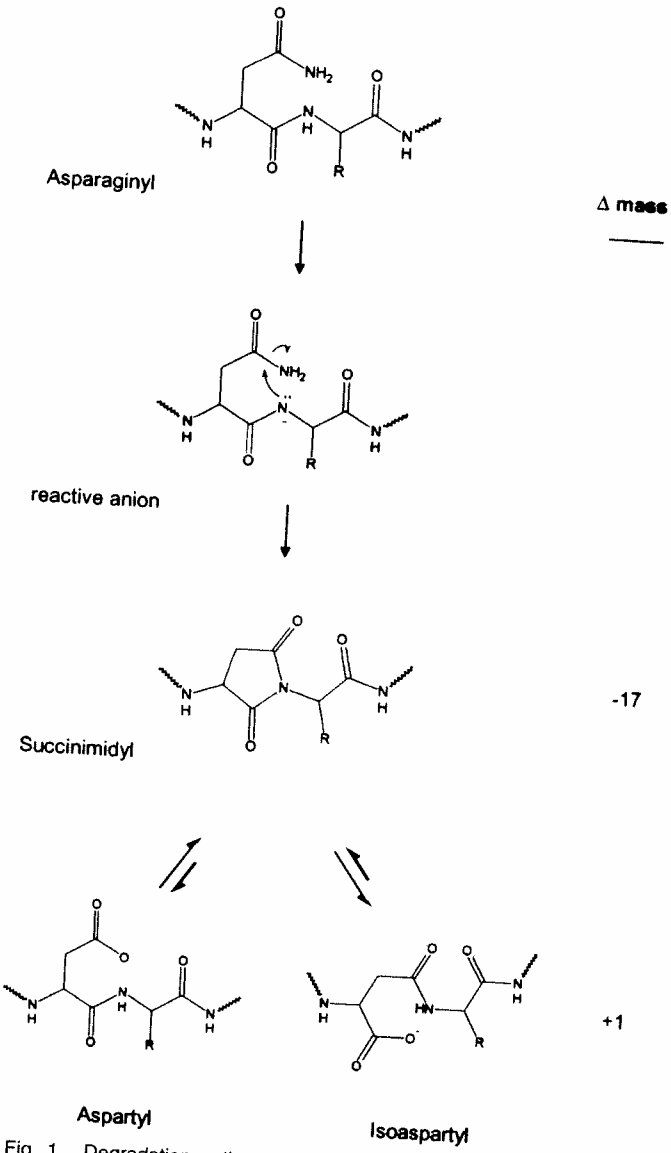

Fig. 1. Degradation pathway for nonenzymatic deamidation of Asn to Asp and isoAsp through the succinimidyl intermediate. Changes in mass from Asn to the intermediate and end products are given.

of its apparent universality, deamidation has been proposed to regulate protein activity and even function as a molecular clock for biological events.[37–39] Because deamidation can cause misfolding and lead to further degradation, such as aggregation[48] or altered immunogenicity,[55] a sensitive commercial assay based on PIMT[43,56] is commonly applied to test purified proteins for the presence of isoAsp itself and as an indirect indicator of deamidation. This assay has been particularly useful in the characterization and quality control of manufactured recombinant proteins.[31,42,43] However, detection of total isoAsp does not reveal the source, number, or site of modification because it measures the combined contribution from spontaneous Asp isomerization as well as from Asn deamidation, each site of which differs in reaction rate and fractional yield of isoAsp. Moreover, the assay reveals nothing of Gln deamidation, which can be prevalent in some proteins.[36,57–59] A computational algorithm that has so far predicted rates of deamidation with remarkable accuracy from amino acid sequence and known three-dimensional structure[60] is commonly applied in support of, and often in lieu of, experimental data. Nevertheless, only direct detection and measurement of site-specific modification provides actual and specific knowledge of protein deamidation.

Mass spectrometry (MS) can detect the ~1 Da increase in molecular mass caused by a single deamidation event, and methods have been reported for this purpose using instruments of low and high mass accuracies.[37,40,43,61–66] Instruments with exact mass resolution can measure the 0.019 Da average difference in signatures between a mass shift caused by deamidation (averaging +0.9841 Da) and the that associated with the first heavy peak of an isotopic profile (called "A+1" and averaging +1.003 Da) for any compound containing a heavy isotope of ^{13}C, ^{15}N, ^{2}H, ^{17}O, or ^{33}S (also see www.ionsource.com).[67] Because ordinary MS instruments of nominal resolution cannot directly discriminate between these sources of an apparent ~+1 Da shift in mass,[40,61,63] the amount of deamidation is commonly estimated as the difference between theoretical and observed isotopic profiles. Since theoretical isotopic profiles are speculative, empirical measurements better serve this objective. Therefore, a favored approach is to compare two states of the same analyte for a change in isoform profiles, which requires differential treatment of the protein or peptide under study.[40,61,63] While useful for confirming a single deamidation, these methods are blind to the positioning of multiple deamidations present on a measured peptide. Thus, the site of deamidation cannot be specified without sequence verification using Edman degradation or, more conveniently, tandem mass spectrometry (MS/MS). This gives rise to a second impasse to the precise measurement of deamidation: that common mass-based sequence alignment tools do not accurately assign the occasional detection of an A+1 isotopic species, and often misappropriate the excess mass to deamidation where plausible. Such an error does not occur during the evaluation of other post-translational modifications in which the modified mass is not similar to the first heavy peak of an isotope profile. The error in automated discrimination between deamidation and the A+1 peak becomes substantial when an observed +1 delta mass deviation aligns with a putative Asn or Gln residue whose position in the amino acid sequence is supported by fragmentation product ion spectra. The typical result is an overestimation of potentially deamidated sites by many MS instruments and commercial software in use today. Herein, we describe a simple solution to both of these difficulties, which verifies the site of deamidation and allows semiquantitative estimation of percent modification without relying on subtraction of isotopic profiles. Application of this procedure allowed us to measure, for the first time, the global composition of site-specific deamidation in PA protein, to determine that isoforms are

caused by partial and differential deamidation across seven Asn residues, and to observe direct correlations between their deamidation, isoform complexity, and reduced biochemical and biological activities of protective antigen.

MATERIALS AND METHODS

Biological and Chemical Materials

Four grades of rPA protein were used in this study. Pharmaceutical grade rPA was purified from ΔSterne-1(pPA102) CR4, a nonsporogenic avirulent expression strain of *B. anthracis*,[68,69] by contract (Biopharmaceutical Development Program, SAIC-Frederick, MD) under good manufacturing practices (GMP), using a proprietary procedure derived from the discovery-based method.[70] This GMP grade rPA was supplied in vials as bulk substance at 1.18 mg/mL and 94.6% purity, in 50 m*M* ammonium acetate at pH 8.9. Intentionally degraded rPA protein of the same GMP lot was achieved through exposure to multiple cycles of freeze, thaw, and hold at 4°C. Research and development (R & D) preparations of rPA were purified from culture supernatants of the same *B. anthracis* expression strain, essentially as published,[70] except pools differing in isoform content were collected as separate fractions across the primary peak of the second step in the sequential process, and held frozen at −70°C until this study. Commercial grade rPA was purchased as a lyophilized preparation and resuspended in water just before use as directed by the manufacturer (List Biologicals, Campbell, CA). LF was prepared as described.[4] Sequencing-grade trypsin was from Promega (Madison, WI). Chymotrypsin and V8 (endoproteinase Glu-C) were from Sigma (St, Louis, MO). Synthetic peptides were from New England Peptides (Gardner, MA), and comprised the native (IAFGFNP*N*GNLQYQGK) and fully deamidated, PIMT-corrected (IAFGFNP*D*GNLQYQGK) mimetics of the PA tryptic peptide 529–545. HPLC-grade acetonitrile with formic acid (LC-MS CHROMASOLV®) and all other chemicals were from Sigma. Sterile, deionized water was polished in the laboratory by a Solutions 2000 water purification system (Aqua Solutions, Jasper, GA).

Capillary Isoelectric Focusing

The isoelectric point (pI) of each measurable rPA protein isoform was obtained by capillary isoelectric focusing (CIEF) using reagents and software of the BioFocus instrument as described by the vendor (Bio-Rad, Hercules, CA). Relative mobility (R_m) of proteins used to construct the standard curve was calculated by using the formula: $R_m = (t_p - t_c)/(t_a - t_c)$, with analyte migration time denoted as "t_p" for protein standard, "t_c" for cathode interface, and "t_a" for anode interface. Theoretical pI values were calculated from the substitutions of the PA amino acid sequence (P13423),[71] as adjusted *in silico* to omit the 29 amino acid leader sequence using the protein parameters tool of ExPASy (www.expasy.org).

Polyacrylamide Gel Electrophoresis

rPA was fractionated on native PhastGels (Amersham Biosciences, Piscataway, NJ) as described previously,[23] employing multiple loadings of 2 μg per lane to purify isoforms for LC-MS/MS analysis. Protein isoforms were also fractionated by two-dimensional polyacrylamide gel electrophoresis (2-DE) according to instructions of the instrument and supplies vendor (BioRad, Hercules, CA), loading 12 μg of rPA protein in sample rehydration buffer per duplicate IEF strips of pH ranges 3–10, 4–7, and 4.7–5.9. For second dimension separation, the developed IPG strips were equilibrated as prescribed, then loaded onto Bis-Tris XT Criterion gels (4–12%, IPG well +1), processing six gels simultaneously (including replicates) in a DodecaCell apparatus at 200 V for 45 min with MES running buffer system.

For imaging and protein excision, gels were washed in deionized water and stained with GelCode blue (Pierce) according to vendor instructions. Images were captured with a FlouS Max2 (BioRad, Hercules, CA) and spot patterns analyzed using PDQuest version 7.1. Orthologous protein isoform spots from replicate gels of each separation were selected and excised using the Proteome Works Spot Plus Cutter (BioRad, Hercules, CA), or with a clean razor blade. All gel plugs were processed promptly for in-gel proteolysis and LC-MS/MS analysis.

Mass Spectrometry

Complete amino acid sequencing by LC-MS/MS

The complete amino acid sequence of GMP grade rPA protein was determined from analysis of spectral data collected by LC-MS/MS, as described previously but with some modifications.[72] Protein was digested with trypsin, chymotrypsin, Glu-C, or a combination of these proteases, performed as recommended by the vendor. For protein contained within excised gel pieces, each gel piece was diced into smaller pieces (~1 mm^2), collected into one tube, and washed 3 × 10 min in acetonitrile: 25 m*M* ammonium bicarbonate (1:1), dried under vacuum, then resuspended in 25 μL of 25 m*M* ammonium bicarbonate pH 8.4 to which was added 75 μL (300 ng) of trypsin stock (Promega), prepared previously by suspending the enzyme in 25 m*M* ammonium bicarbonate at 4 μg/mL and stored at −20°C as recommended. Fragments were recovered in gel supernatants and combined with two consecutive extractions of the gel pieces with 100 μL of 50% acetonitrile, 0.1% formic acid. The pooled extracts were dried under speed vacuum and reconstituted in 30 μL of 5% B chromatography buffer. Samples were transferred to 1.1-mL crimp-capped vials with 400-μL volume inserts (PN 9301-1388, Agilent Technologies, Wilmington, DE) and stored at 4°C for analysis by LC-MS/MS within 24 h. For direct proteolysis of free protein in solution, the process was carried out as recommended by protease vendors (18 h, 37°C) using 11–15 μg of rPA protein (enzyme/protein ratio of 1:15-20, w/w). The reaction was stopped with 4 μL of formic acid. Final injected

amount of 28 μL contained a calculated 4.96–5.43 pmol of digested protein. Importantly, since rPA contains no cysteines, protein and peptide samples were not denatured, reduced, or alkylated in these studies, whether for analysis of amino acid sequence or analysis of post-translational modification. This precaution was applied to limit sample exposure to conditions that enhance Asn deamidation, specifically the high ionic strengths of guanidine hydrochloride, dithiothreitol, and iodoacetemide.[66,73]

After collection, mass spectral data were analyzed in two stages to verify total amino acid sequence. First, the spectral data were parsed against a custom database containing only the rPA amino acid sequence. Filters of the Spectrum Mill search engine (Agilent Technologies) were set to allow up to five missed cleavages, passing peptide scores greater than 15 in combination with SPI (scored peak intensity) greater than 70%. These criteria returned results of high confidence and such peptides were considered to be authenticated ("validated" by software nomenclature). In the second step, poorer quality matches of lower SPI and peptide scores were analyzed with instrument LC software (ChemStation, Agilent) and manual inspection. Both precursor and product ions were confirmed and the validity of the peptide was decided based on manual inspection of peaks. The product ion peaks that showed little fragmentation or few matching fragmentation were removed from the lists of validated peptides.

Instrument and system set-up for collection of deamidation spectra

An Agilent 1100 Series LC/MSD Trap SL was equipped with an electrospray ionization (ESI) source to analyze peptides separated on a Zorbax Stable Bond column (SB-C8 2.1 × 150 mm^2, 3.5 μm narrow-bore column) maintained at 40°C and operated with running buffer A (0.1% formic acid) and premixed running buffer B (0.1% formic acid in acetonitrile). LC method: 200 μL/min; 28 μL/injection; gradient from 5% B to 45% B over 50 min. The MSD method: positive polarity with ICC parameters of 100,000 target value, 300.00 ms maximum accumulation time at 300–1800 m/z scan range with three averages; Normal scan resolution (13,000 (m/z)/sec); 40 psi nebulizer; 10 psi drying gas, 350°C capillary temperature, Smart Parameter settings of 920 m/z target mass, 100% compound stability, 140% trap drive, normal optimization; autoMS(n) on, 0.15-min cycle time, two precursor ions, 25,793 threshold absorbance, 5% threshold relativity, preoperation SPS, acquisition parameters of 1.30-V fragmentation amplitude, with Advanced settings preference for doubly charged precursor ions and group length of five, and Acquisition Parameters of 10 scan averages at maximum resolution, 5 MS(n) averages, and 4.0 m/z isolation width. Background ions were excluded from MS(n) analysis as determined empirically.

Verification of deamidation and other amino acid modifications

For each peptide that was flagged by automated analysis to possibly contain modified amino acids, raw spectral data were inspected manually against an rPA custom database using Spectrum Mill entries for modifications of Gln and Asp deamidation, succinimidyl intermediate, methionine oxidation, N-terminal acetylation and carbamylation to confirm or refute the corresponding change in mass for the appropriate amino acid substitution according to the following step-wise verification procedure: (1) Preference was set for precursor peptide ions of +2 charge, but triple charge ions were used when at least two fragmentation ions were observed with the expected masses and none with a contradictory mass; (2) The extracted ion chromatogram (EIC) for each of these confirmed peptides was plotted by instrument software to confirm multiple forms. The observed precursor ion using mass ranges according to specific modification and ion charge are as follows. Specifically, most analyses concerned the doubly charged deamidated peptide ions having a delta mass of +1 ($\Delta\ m/z = +0.5$). The EIC range for detecting Asp or isoAsp deamidation products was set as follows: range A = [(precursor mass +1)/2−1 to (precursor mass +1)/2 + 4)]. However, for analysis of peptide L450-R468 which contains one succinimide, doubly charged peptide ions having delta mass of −17 ($\Delta\ m/z = -8.5$) employed different EIC limits: range B = [(precursor mass −16)/2 − 1 to (precursor mass +1)/2 + 6]. Analysis of peptide E704-K722 carrying two sites of modification utilized triply charged succinimide peptide ions, also having a delta mass −17 (but $\Delta\ m/z = -5.66$), used range C = [(precursor mass −15)/3 − 1 to (precursor mass +2)/3 + 2]. The triply charged ions were used here because they fragmented better and provided peak intensities 15–22 times greater than those observed for doubly charged ions, enabling better area calculations. Peptides that did not show evidence of succinimide intermediate were extracted using a range that contained both native and deamidated peaks and doubly charged peptides. Every site was examined for the presence of LC-separated precursor peptide ions, two peaks for native versus deamidated, and to two more peaks for iso-Asp and succinimide. Differential reversed phase (RP-HPLC) retention between the native and modified states was observed for every peptide carrying a confirmed deamidation, although not every deamidation showed iso-Asp or succinimide forms. Potential assignments showing a single EIC peak were eliminated; and (3) The y and b product ions of MS/MS spectra for each precursor peptide were viewed along successive overlapping fragments to confirm that the +1 Da mass shift (Asp or iso-Asp), or −17 Da mass shift (succinimide), aligned with the residue expected to be modified, concurrently also confirming all surrounding amino acid sequences sequence on that peptide. Rare isobaric precursor ions found to be peptides of wholly different amino acid sequence were eliminated from further consideration. Sim-

ilar methodology was applied to confirm Met oxidation but using a delta mass of +15.99 Da.

Measurement of absolute deamidation and calculation of percent deamidation

Once native and deamidated residues were confirmed and verified in association with separated precursor ions, the absolute amounts of native and deamidated species were estimated by integrating the peptide EIC peak with instrument default settings. Peak areas were calculated from the peptide precursor ion EIC using the monoisotopic mass with custom range window (ranges A, B, and C specified above) so as to integrate the most intense portions of the isotopic envelope.

Relative deamidation at each confirmed site was then calculated from EIC chromatographic peak areas as a percentage, comprising the quotient of the native, or deamidated peptide ion in relation to the sum of areas for all pertinent ions [Eq. (1)],

$$D_i = [(A_{D_i})/(A_{D_i} + A_{N_i})]100 \quad (1)$$

where D_i is the percent deamidation calculated at position i, A_{D_i} is the peak area of the precursor ion confirmed to be deamidated at position i by containing Asp in place of the expected Asn, and A_{N_i} is the peak area of the precursor ion confirmed to be native by containing Asn at position i, and all residues of the peptide outside position i confirmed according to expected amino acid sequence. Where observed, A_{D_i} also included EIC peak areas for isoAsp or succinimide, typically situated before the Asn peak and after the Asp peak, respectively, due to differing retention times by RP-HPLC.[66] Percent deamidation at Gln is calculable by a corresponding equation, but was not needed as Gln deamidation was not observed in rPA. The same basic equation was used to measure percent oxidation of Met.

Biochemical and Biological Activities

Native PhastGels were used to evaluate the ability of furin to cleave different preparations of PA_{83}, of cut PA_{63} to assemble into $(PA_{63})_7$ heptamers, and of the heptamer to bind LF in forming the $LF(PA_{63})_7$ holoenzyme complex, as previously described.[21] The biological activity of various preparations of rPA to function in association with LF as anthrax lethal toxin, $LF(rPA_{63})_7$, was tested by measuring the viability of macrophage cells after exposure, in an improved method originally reported by Friedlander.[74] Dilutions of rPA were prepared in triplicate and combined with 40 ng/mL of LF (final concentration) in cell culture-treated, 96-well Costar plates (Corning Incorporated, Acton, MA). Dilutions were prepared in Dulbecco's Minimal Essential Medium Complete, i.e., with the following additions: high glucose (Invitrogen-Gibco, Gaithersburg, MD) containing 7.5% heat-inactivated fetal bovine serum, 25 m*M* HEPES, 4 m*M* glutamine, 100 μg per mL of streptomycin, and 100 U per mL of penicillin. One-hundred microliters per well was then transferred to cell culture-treated 96-well plates seeded with 5×10^4 of J774A.1 cells in 200 μL volumes 18–22 h before testing after removing the culture medium. Cells were maintained in Dulbecco's Minimal Essential Medium Complete without 25 m*M* HEPES. After incubating the plates for 4 h in a humidified incubator set at 37°C and 5% CO_2, 25 μL per well of 3-[4,5-dimethylthiazol-2-yl]2,5-diphenyltetrazolium bromide (MTT) at 5 mg/mL of PBS was added and the plates reincubated for 2 h. Cells were then lysed and the insoluble reduced formazan was made soluble by adding 100 μL per well of lysing-solubilization buffer.[75] After an overnight incubation, the absorbance values at 570–690 nm for each well were collected by using a BioTek 312e microplate reader (BioTek Instruments, Winooski, VT). The protein concentration of each PA test sample that resulted in 50% killing of cells in the presence of LF was calculated (EC_{50}) using the 4-parameter logistic regression analysis of SoftMax Pro (Molecular Devices, Sunnyvale, CA).

Computational Methods

Predicted rates of Asn deamidation in the monomer were calculated using the algorithm of Robison and Robinson available at www.deamidation.org. Correlations between percent deamidation and negative charge or biological activity were calculated using the Pearson product-moment correlation in SAS software, Version 9.1 (SAS Institute, Cary, NC). Modified amino acids of PA monomer and heptameric PA prepore (PDB code 1ACC and 1TZO) were viewed and studied using Open-Source PyMOL™ Version 0.97 (www.pymol.org) (DeLano Scientific LLC, SanCarlos, CA).

RESULTS AND DISCUSSION

Visual Analysis of PA Isoforms Indicates Rapid Protein Modification *in vivo*

Almost two decades ago, Leppla[4] reported the existence of natural PA protein variants during the first isolation and characterization of *B. anthracis* exotoxin proteins. PA heterogeneity appeared as micro-charge isoforms of incrementally greater negative charge, as first detected by ion exchange chromatography and nondenaturing slab gel electrophoresis.[76] These isoforms were subsequently characterized in detail with CEIF (Fig. 2), native PhastGel[23] (Fig. 3), and 2-DE (Fig. 4). Because isoforms of natural and rPA were all seen to share the expected M_r of 83 kDa,[4,23,70] it was suggested that heterogeneity could be caused by post-translational modification, most fittingly deamidation.[23] Although supportive evidence for deamidation was recently reported,[23,63] this hypothesis was difficult to prove due to the small associated delta mass and was not definitively and specifically demonstrated for PA protein until this work, as described herein. First, we considered how, in light of certain evidence for deamidation, the evaluation of visible isoforms revealed two unexpected details of rPA

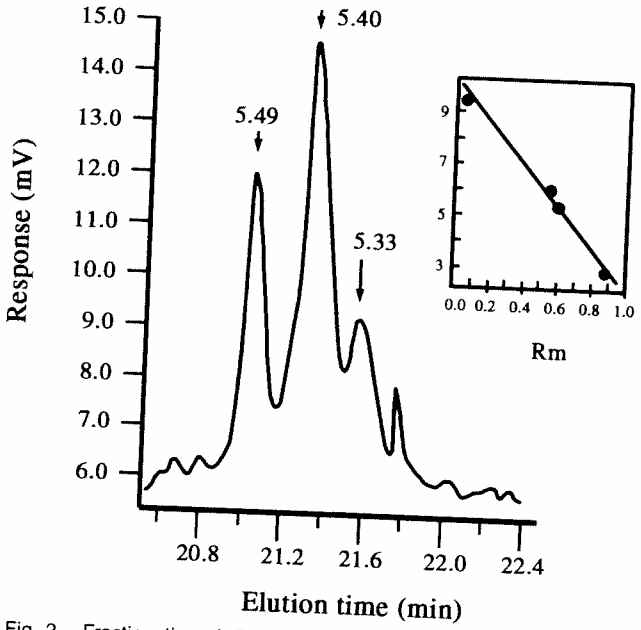

Fig. 2. Fractionation of rPA isoforms by CIEF. Isoform classes in an R & D lot of purified rPA protein are visible as distinct peaks. Measured pI values, calculated as described in Experimental Procedures, for the three largest peaks are marked by arrows. Inset: standard curve having y intercept = 10.24, slope = −8.0423 and R^2 = 0.9928. The mobilities and pIs of analytes used in constructing the standard were as follows: cathode interface, 9.15 min; RNAse A, pI 9.5, 11 min; carbonic anhydrase isoform, pI 5.9, 23.5 min; carbonic anhydrase isoform, pI 5.4, 24.3 min; CCK flanking peptide, pI 2.75, 31.6 min; anode interface, 34 min. R_m (migration time for peak of interest)/(migration time for salt front) values for rPA sample employed reference interfaces of T_c = 8.56 and T_a = 29.91.

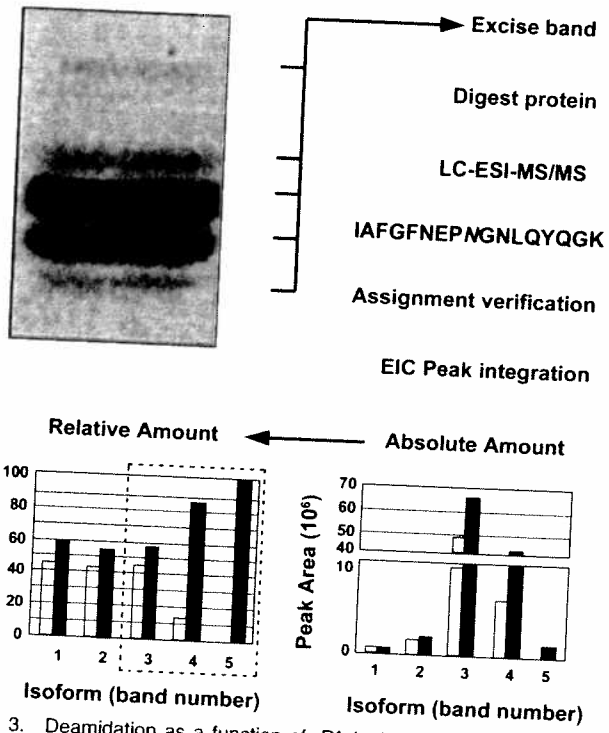

Fig. 3. Deamidation as a function of rPA isoform net charge. Upper left, coomassie blue-stained native PhastGel of GMP grade rPA protein provided isoform bands of increasing negative charge, numbered sequentially from 1 to 5 from top to bottom, which were excised for analysis as summarized in the upper right. Tryptic peptide 529-545 was inspected for deamidation at position N537 yielding: Lower right, absolute levels of modification; and, Lower left, relative amounts of modification. Values (ordinate) for native (light bars) and deamidated (dark bars) Asn537 are plotted as a function of each isolated isoform band from 1 to 5 (abscissa).

protein degradation: that modification occurred very early during protein preparation and that the final state of purified rPA contained substantial modification.

Fractionation by CEIF of purified R & D grade rPA protein showed four clear chromatographic peaks, two dominant and two minor (see Fig. 2). However, peak skewing and shouldering indicated incomplete separation and the probable existence of additional minor coeluting and unresolved species. The three most abundant CEIF isoforms each differed in pI by ~0.1 pH unit, and all values were close to (within 0.55 pH unit), but measurably less, than the calculated pI of 5.88 for rPA.[71] Native PhastGel analysis was developed as a convenient and robust assay of protein purity and quality in the production of pharmaceutical grade rPA protein manufactured under GMP controls for testing rPA as the next anthrax vaccine antigen.[23,24,70] Method optimization through process development finally reduced the number and apparent intensities of visible charge-class species (isoform complexity) in rPA to two principal isoforms with insubstantial contamination. The single most effective procedure used to reduce isoform complexity was the introduction of an early ammonium sulfate cut as a controlled hold step (S. Giardina, unpublished results). This curtailed the accumulation of additional acidic forms visible in various R & D lots, and effectively concentrated the two isoforms which were seen to be universally present in GMP grade and commercial lots of rPA [Figs. 2–4, 5(A), 6(A)]. Separation of GMP grade rPA by native PhastGel produced five visible staining bands. Similar to CEIF, two of these isoforms dominated the total content of the preparation, and two of the three remaining minor isoform bands were less negative in charge and therefore less acidic (Fig. 3). Finally, 2-DE provided greater resolution of rPA isoforms, and showed from 6 to 10 distinct or merging spots depending on the pH range applied and the freshness of the protein sample (Fig. 4). Isoform complexity generally concurred among all of these analytical methods, with each showing that purified rPA contained two principal charge isoforms plus three or more minor isoforms of distinctly different charge. Nuances in isoform pattern and the degree of isoform visibility depended on the method of observation and quality of the protein analyzed. rPA protein that was degraded by intentional treatment showed greater isoform complexity [Figs. 4(B vs. A, D vs. C, F vs. E), 5(A), fresh vs. treated], as did various R & D lots stored frozen since purification [Fig. 6(A)]. The transition in isoforms toward more negative charge in the developmental lots resembled the progressive shift of acidic forms previously observed during fermentation[23,24,70] and during purification of major isoforms used for early

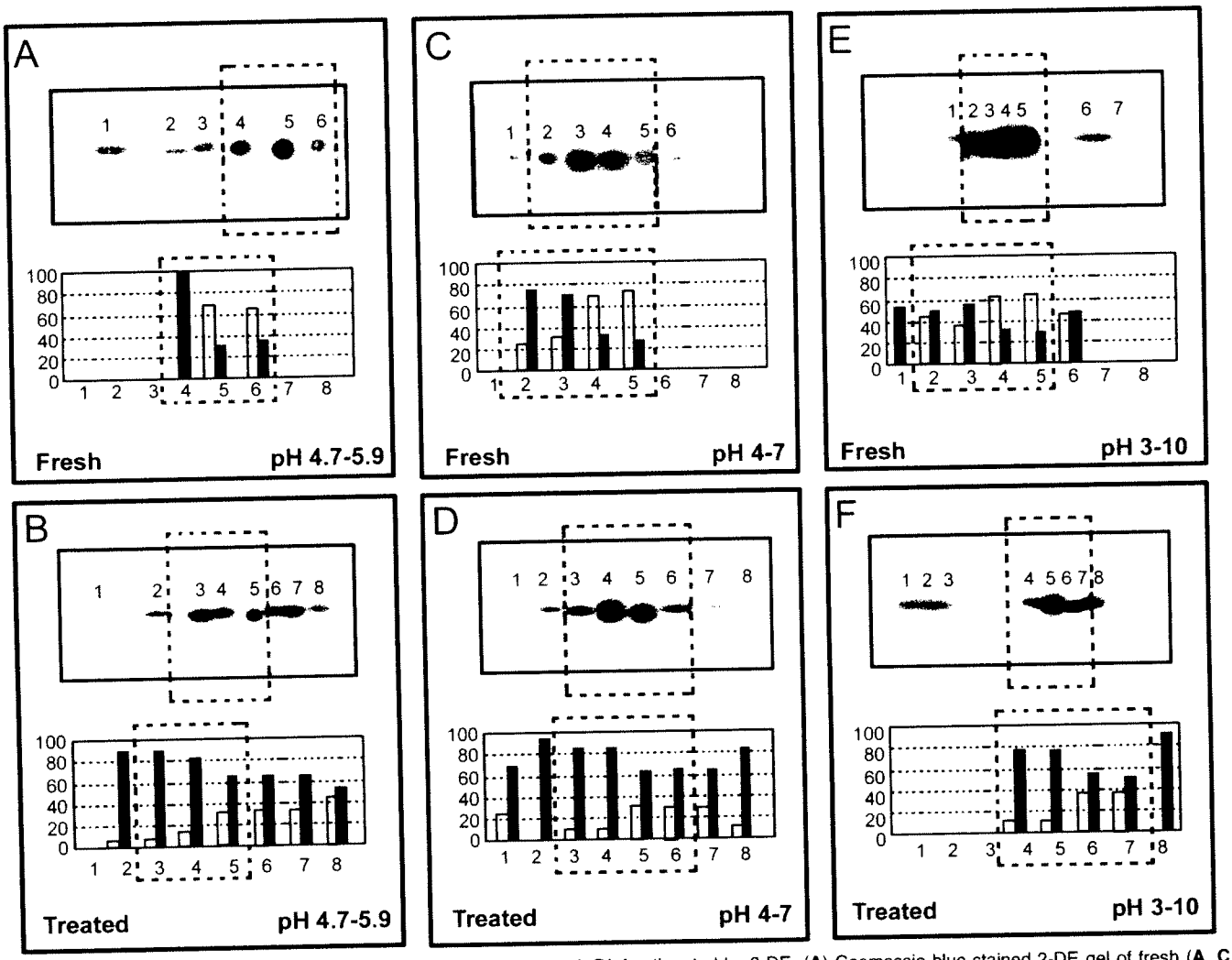

Fig. 4. Deamidation at N537 increases with isoform complexity of rPA fractionated by 2-DE. (**A**) Coomassie blue-stained 2-DE gel of fresh (**A**, **C**, **E**) and aged (**B**, **D**, **F**) GMP grade rPA protein. Gels are oriented with anode on left, and first-dimension pH ranges are shown below each corresponding column. Isoform spots excised and analyzed by LC-MS/MS for deamidation at N537 as contained on peptide 529-IAFGFNEP*n*GNLQYQGK-545 are indicted by histogram bars: dark, deamidated; light, native. Relative ion peak areas (ordinate) are plotted as a function of the isoform spot analyzed (abscissa).

animal vaccination and challenge studies.[23] All of these results clearly demonstrated that isoform complexity increased with protein degradation, decreased with protein purity, and began *in vivo* early during expression. Importantly, each of these techniques revealed the presence of minor rPA species of less negative charge than the components of highest abundance, evident as small peaks preceding the major CIEF peaks (Fig. 2), minor bands above the major PhastGel bands (see Fig. 3), and minor spots of higher positive charge than the major 2-DE spots [Fig. 4, e.g., panel (D) spots 7 and 8]. Review of rPA molecular charge heterogeneity by these three fractionation techniques, and by preparative ion exchange chromatography reported earlier,[23,70] confirmed that the primary forms of purified PA were not the isoform species of least net negative charge, and consequently, were not the least modified form of PA. Thus, by the following reasoning, we conclude that most GMP grade PA protein is modified *in vivo*, and largely to the extent apparent *in vitro* after purification.

First, the two principal isoforms predominated in all preparations but did not comprise the entire content of any purified rPA preparation. These isoforms were seen to dominate rPA isoform populations from the earliest point of detection during fermentation,[23,24,70] and for this reason they were previously designated "isoform 1" and "isoform 2."[23] While these two isoforms together comprise 99.72% of the total protein in GMP grade rPA,[24] and likely as much of high purity rPA produced by a commercial vendor [List Biologicals, Fig. 6(A)], they were also accompanied by very faint, less acidic isoforms as was apparent in freshly thawed GMP grade protein (Figs. 3 and 4), aged GMP protein [Fig. 5(A)], rPA produced by a commercial vendor [Fig. 6(A sample a)], as well as R & D lots of rPA [Figs. 2, 6(A samples b–d]. Because isoforms ostensibly represent incremental post-translational modi-

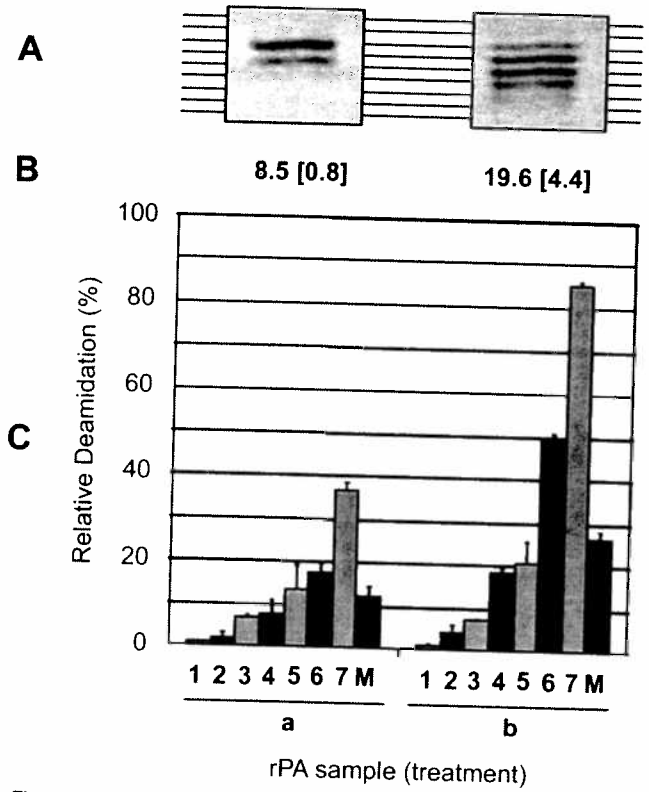

Fig. 5. Multiple-site deamidation and decreased biological activity correlate with increased isoform complexity of aged GMP rPA. Comparison of isoform complexity and biological activity with percent deamidation at seven Asn sites in freshly thawed versus aged GMP rPA. (**A**) Native PhastGels of whole GMP rPA protein; Left, freshly thawed protein; Right, accelerated aged protein. Horizontal guide lines aide in comparing vertical positions of protein isoforms between gels. (**B**) Biological activity measured as EC_{50} (ng/mL) with standard deviation in brackets. (**C**) Relative deamidation measured in each protein sample (abscissa) expressed as percent deamidated (ordinate). Samples, vertically aligned with gel images in A, comprise: a, freshly thawed GMP rPA; b, treated for accelerated aging. Residues: 1, N602; 2, N408; 3, N719; 4, N601; 5, N466; 6, N713; 7, N537; M, mean.

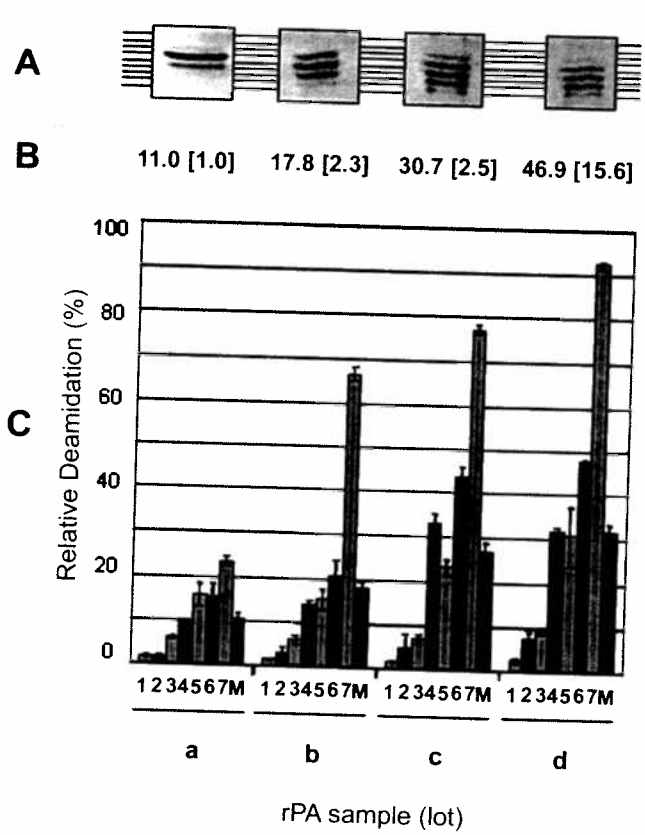

Fig. 6. Multiple-site deamidation and decreased biological activity correlate with increased isoform complexity of different rPA preparations. Comparison of isoform complexity and biological activity with percent deamidation at multiple Asn sites in different rPA preparations. (**A**) Native PhastGels of whole PA protein preparations as designated below. Horizontal guide lines aid in comparing vertical positions of protein isoforms between gels. (**B**) Cytotoxic activities of same PA preparations given in EC_{50} (ng/mL) with standard deviation in brackets. (**C**) Relative deamidation for seven Asn residues in each protein preparation (abscissa) expressed as percent deamidated (ordinate). Samples, vertically aligned with gel images in A, comprise: a, List Biologicals; b, R & D rPA lot 121096a; c, R & D rPA lot 121096b; d, rPA lot 022795b. Residues: 1, N602; 2, N408; 3, N719; 4, N601; 5, N466; 6, N713; 7, N537; M, mean.

fications that impart progressively greater negative charge, the less negative isoforms were presumably less modified (i.e., more native) than the dominant and highly visible isoforms. Second, the uppermost prominent isoform in all final preparations coaligned by native PhastGel, as seen by comparing isoform distribution among R & D lots, the GMP rPA lot, and a lot produced by a proprietary and possibly different process [Figs. 5(A) and 6(A)]. Therefore, these prominent bands had the same net molecular charge. Third, this same predominant upper isoform band [band 3 in Fig. 3(A)] aligned with the upper most prominent band visible in the earliest stages of expression sampled during fermentation, previously called "isoform 1" and shown in Figure 1 of Ribot et al.[23] Therefore, the putative modification causing this isoform occurred naturally and rapidly during expression in the bacterium. Fourth, this same uppermost dominant isoform of rPA had a measured pI value notably less than that calculated *in silico* (5.49 vs. 5.88), was preceded by two minor isoforms of observed pI closer to the calculated value, and was succeeded by isoforms with increasingly acidic pI values (Figs. 2 and 3). Thus, most of the PA protein produced during expression and present after purification exhibited charge states that were more acidic (negatively charged) than those calculated from amino acid sequence and were therefore more modified than nascent rPA protein. Finally, in every preparation we studied, the trend of increasing isoform complexity comprised an acidic shift in isoform distribution beyond that of the principal isoforms, whether observed during bacterial growth, collected as fractions across a primary peak during isoform purification,[23] created inadvertently through handling or extended 4°C hold during process development [Fig. 6(A)],[70] or intentionally produced by freeze/thaw/hold cycling to achieve accelerated aging [Fig. 5(A)]. We conclude that PA protein was rapidly and naturally converted to several successively acidic states *in vivo*, two of which predominated and were enriched during purification. All of these findings are concordant with the

earlier suggestion that the probable cause of PA heterogeneity is multiple-site, amino acid deamidation.[23] Two opposing explanations concur with these findings: either the principal components were not fully native and negatively charged modifications were the only alteration present, as proposed here, or there may have also been hypothetical modifications imparting positive charge. We offer direct and definitive proof for the first hypothesis. Such evidence required the development of a robust LC-MS/MS method for detecting and inspecting every site of deamidation with an empirical approach for their qualitative and semiquantitative analysis. With these tools, gel-isolated isoforms were inspected for variation in deamidation in relation to isoform complexity to define the chemical source of PA heterogeneity.

Complete Amino Acid Sequencing of rPA Protein by LC-MS/MS

Evaluation for deamidation began with the complete sequencing of rPA by MS. Analysis of MS/MS spectral data for GMP protein digested with trypsin, chymotrypsin, Glu-C (V8 protease), or combinations of these three proteases, and parsed automatically against a custom rPA database confirmed 86% of the predicted amino acid sequence. Four expected peptides were not observed within set limits of the mass analysis program including 22-YSFDLNFQAPMVVTSSTTGDLSIPSSELENIPSENQY-FQSAIWSGFI-KVK, 111-GRLYQIKIQY, 133-K, and 158-QKSSNSRKK. However, we were able to detect and fragment these peptides and extend amino acid sequence coverage to 100% by eliminating the peptide ion matching tolerance limits, instead using instrument software and manual inspection to confirm these ions (see Materials and Methods). Merging of all data resulted in total amino acid sequence confirmation with the observation of every possible source for deamidation, as shown in Figure 7. All 68 Asn residues and all 30 Gln residues were observed, and those showing mass deviation were inspected for confirmation as being either native or deamidated through redundant mass-based amino acid sequence analysis with manual verification. Automated analysis of the spectral data flagged 61 Asn and six Gln for potential deamidation, plus one Met for potential oxidation (Fig. 7). However, most of these flagged modifications were erroneous assignments, as determined by the verification process discussed next. No deletions were detected, and a directed search for other possible amine-specific modifications listed in the search engines revealed no other post-translational modifications.

A Simple Method to Verify Deamidation: Demonstration of Site Specific and Multiple Asn Deamidation in PA

While the previously reported enzymatic detection of isoAsp provided strong supportive evidence of deamidation in PA,[23] it did not confirm the existence of deamidation or reveal its nature. Alternatively, MS techniques such as MALDI-TOF-MS that do not preseparate peptide

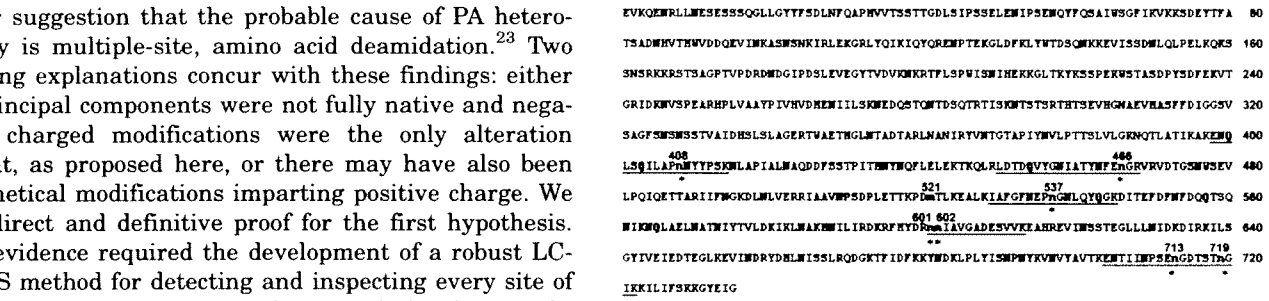

Fig. 7. Summary of LC-MS/MS analysis of rPA for amino acid sequence and post-translational modifications. Shown is the amino acid sequence of rPA (accession P13423) as experimentally verified by LC-MS/MS in universal single letter code, beginning with the N-terminal amino acid remaining after natural removal of the leader sequence (i.e., PA_{83}). Special nomenclature and markings as follows: **n**, Asn residue, identified by coordinate, experimentally confirmed to be partially deamidated by also containing Asp; **m**, residue observed to be partially oxidized by also containing oxyMet; **bold type**, amino acid sites predicted to be modified by automated MS/MS analysis; solid underscore (_), tryptic peptides containing 7 confirmed sites of deamidation; superscript number and asterisk (*), residue coordinate confirmed to be modified as described in Experimental Procedures. Findings are compiled from data collected and analyzed on fragments from digestion with trypsin, chymotrypsin, or endoproteinase Glu-C (V8 protease) of GMP rPA as described.

forms by LC or analyze ion composition by MS/MS fragmentation can confirm deamidation but cannot discriminate the location, nature, or quality of the putative amino acid deamidation. Calculation of deamidation by such methods rests on comparing isotope peak abundances between the monoisotopic A peak and all major peaks of the isotopic series, which principally includes the A+1, A+2, A+3 peaks for average-sized peptides. However, this measurement of peak abundances is only provisional without better than 5 millimass unit accuracy or certain knowledge of elemental composition. This is because the A+1 ion of the ^{12}C form for a truly deamidated peptide ($\Delta\ m = +0.9841$ Da for a single Asn deamidation) and the first heavy isotopic form of the native peptide (e.g., $\Delta\ m = +1.003$ Da for a single ^{13}C) are collected together within the same m/z range window during a time of flight mass spectrometry experiment. Without high mass accuracy measurement, the resulting over-representation in A+1 peak area must be assumed as constant between differentially treated samples. Moreover, this method cannot distinguish multiple deamidation present on the same peptide.

In contrast, we optimized a simple LC-MS/MS method to definitively ascribe an observed +1 Da mass shift to deamidation at a specific amino acid residue, even using an instrument of 0.2 m/z nominal mass accuracy. This method of verification was based on satisfying three criteria for every deamidation while inspecting raw spectra: criterion (1) the presence of resolved RP-HPLC peaks for all variants of the deamidated peptide in question, with delta mass of +1 Da (Asp, isoAsp, Glu) or −17 Da (succinimide); criterion (2) confirmation among fragmentation ions that each mass shift aligned with the suspected modified residue in the observed peptide amino acid sequence; and criterion (3) confirmation that the monoi-

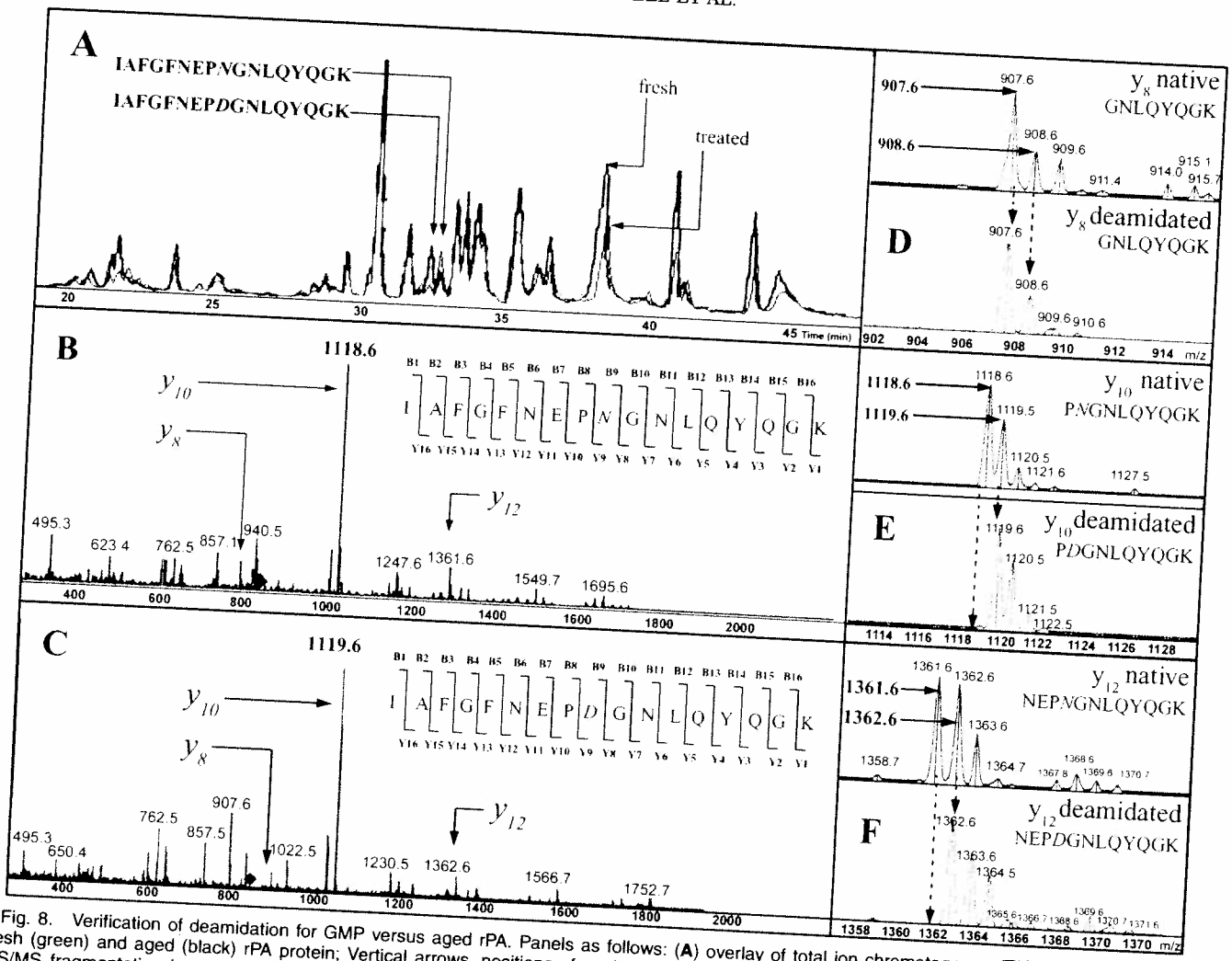

Fig. 8. Verification of deamidation for GMP versus aged rPA. Panels as follows: (**A**) overlay of total ion chromatograms (TIC) of tryptic digests of fresh (green) and aged (black) rPA protein; Vertical arrows, positions of peaks for tryptic peptide 529–545 carrying native or deamidated N537. (**B**) MS/MS fragmentation ions of doubly charged native precursor ion 949.5 (blue diamond), R.T. 32.4 min. (**C**) MS/MS fragmentation ions of doubly charged native precursor ion 950.0 (blue diamond), R.T. 32.7 min. (**D**) Zoomed in view of y_8 peaks confirming N539 is native Asp. (**E**) Zoomed in view of y_{10} peaks confirming N537 is deamidated; note that monoisotopic y_{10} MS/MS fragmented mass shifts from 1118.6 to 1119.6. (**F**) Zoomed in view of y_{12} peaks concurring with deamidated N537 and native N534; Y_{12} fragment mass ion only shows +1 mass shift from 1361.6 to 1362.6. Panels d–e: blue curve, native peptide; red curve, deamidated peptide.

sotopic peak was used for every mass assignment. This method of quality control was performed for each potentially deamidated site that was automatically flagged during initial sequence confirmation. A schematic outline of the overall approach as applied for gel-isolated protein isoforms is shown in Figure 3. A representative example of this MS process is illustrated in Figure 8 which compared fresh versus aged rPA: panel A for criterion 1; panels B and C for criterion 2; and panels D–F for criterion 3. Note that as part of criteria 2 and 3, the mass shift did not appear on fragmentation product ions that did not contain the site of deamidation, as exemplified by ion y_8 in Figure 8, panel D. Thus, the site of deamidation was confirmed by the observations of a +1 Da mass shift on successively longer product ions containing the residue in question, of native masses for successively shorter product ions not containing the questioned residue, and of all other ion data that conformed to the expected amino acid sequence.

By this method, spectral data for the entire amino acid sequence of GMP grade rPA were inspected and verified for sequence and post-translational modifications. Seven Asn residues situated on five tryptic peptides were confirmed to contain deamidation: N408, N466, N537, N601, N602, N713, N719 (Fig. 7). While deamidation was also detected at an eighth flagged site, N539 (i.e., two EIC peaks and confirmatory y product ions), the EIC peak areas were too small to calculate absolute, even on samples of high isoform complexity, so this site was provisionally designated as unmodified. The six Gln automatically flagged for deamidation were all found to be native (Q400, Q403, Q454, Q543, Q557, Q565, Fig. 7). In each of these automatically generated mis-assignments, the software had erroneously employed an ion's

 DOI 10.1002/prot

A+1 peak in assigning its monoisotopic mass. Inspection of the single flagged Met (M521) using a mass shift of +15.99 Da for oxy-Met sulfoxide confirmed it was partially oxidized, with 1.43% oxyMet content measured in fresh protein (Table I). The amount of oxyMet did not increase with treatment (Table I).

In summary, we found that GMP grade rPA protein contains seven Asn residues with detectable and quantifiable deamidation (Fig. 7), plus an eighth site just barely detectable but too low to quantify. The only additionally observed modification was a slight oxidation at a single Met, and oxyMet does not impart a charge to the protein. These data provided definitive, comprehensive, and specific chemical support for the long speculated but unproven hypothesis that PA protein isoforms are caused by amino acid deamidation. Interestingly, none of these seven sites was seen to be fully modified, and each varied in content according to isoform complexity, as discussed below.

Demonstration of absolute and relative deamidation: cataloging fractional deamidation in purified rPA protein

After establishing all sites of modification and observing only partial levels of deamidation in every case, we explored whether these data could provide an empirical measure of absolute deamidation. While inspecting raw LC-MS and MS/MS data to verify site specific deamidation, we observed that most peptide variants were sufficiently separated by LC before mass analysis, and so it became evident that the amount of deamidation could be estimated by direct integration of EIC chromatographic peak areas instead of the typical method of calculating differences between observed and inferred isotope peak profiles. The absolute amount of each peptide form was measured independent of its comparative variant of interest, and relative levels of deamidation were calculated directly from these empirical values. Thus, this method circumvented common calculations that gauge comparative peak areas derived from theoretical isotopic profiles or from differentially treated samples.[61,63] Furthermore, because RP-HPLC separates peptides according to hydrophobic character and not mass [criterion 1, illustrated in Fig. 8(A)], observed peptide isoforms of +1 delta mass comprised only the deamidated species and not a heavy version (e.g., ^{13}C) of the native species [criterion 3, illustrated in Fig. 8D–F]. In this method, isotope analysis was used only to support the interpretation of MS/MS fragmentation data in confirming the identity, purity, and correct mass assignment of each peptide ion. Calculations across all confirmed sites of modification in rPA confirmed differing levels of partial deamidation, and in no case was a native peak absent (i.e., 100% deamidation), including peptide 529–545, which carried the Asn of highest observed deamidation [Figs. 5(C) and 6(C)]. The clarity of measuring deamidation in this manner is visually illustrated in Figure 8 for this same peptide, wherein freshly thawed GMP grade protein had a larger native N537 peak (peptide isoform containing only Asn at position 537) than did treated protein, while the treated protein had a larger deamidated peak (peptide isoform containing only Asp at position 537) than did fresh protein. As calculated from only confirmed peak areas using Eq. (1), the measured percent deamidation at this site was 35.5% in fresh protein and 85.2% in treated protein [Fig. 5(C), Table I]. The presence of both native and deamidated forms of a peptide separated by charge via LC before mass analysis [Fig. 8(A)] was observed for every proteolytic fragment carrying a confirmed Asn deamidation. However, before measuring each site for absolute and relative deamidation, we first verified that these calculations were reproducible using model synthetic peptides of differentially defined composition as follows.

While electrospray ionization MS can provide quantitative measures of ions within certain density ranges of the instrument ion trap, we nevertheless tested the hypothesis that the proposed method could accurately estimate levels of deamidation. For this purpose, we performed measurements on synthetic peptides that mimicked the tryptic fragment containing the site of highest observed deamidation (529-IAFGFNEP*N*GNLQYQGK-545), such that one peptide contained the native form (N537) while the second contained the fully deamidated and PIMT-corrected form (D537). Dilutions and measurements of each peptide in isolation confirmed that a standard curve could be constructed for each peptide with good fit to linearity (native N537 peptide: $R^2 = 0.9975$; deamidated D537 peptide $R^2 = 0.9918$). This linear range encompassed most of the ion intensities observed experimentally for rPA-digested peptides [Figs. 3, 4, 5(C), 6(C), Table I]. Moreover, mixing the two synthetic model peptides in different ratios and measuring them as "unknown samples" demonstrated that their measured fractional compositions aligned with calculated stoichiometric compositions (data not shown). These results confirm the proposal that, at least for these two peptide mimetics of native and deamidated tryptic fragment 529–545, this method dependably and accurately measured the absolute and fractional amounts of deamidation at residue N537. Without specific demonstration, we propose that correspondingly similar representation can be extended to other rPA peptides carrying sites of deamidation. Thus, through direct measurements of separated native and deamidated peptide peak areas, this method provided an estimate of absolute and relative deamidation at every observed modified position without dependence on deduced or differential isotope profiles.

Absolute and relative levels of deamidation were measured across all modified Asn residues in freshly thawed GMP grade rPA protein. All Asn deamidations reacted to a different extent and could be arranged in the following rank order of net conversion to Asp: N537 > N713 > N466 > N719 > N601 > N408 > N602 [Table I, Fig. 5(C)]. Using this single point of observed Asp content as an approximate measure of an Asn residue's propensity to undergo deamidation, these data appear to differ from the rank order for rates of deamidation predicted by the

TABLE I. Summary of Observed Amino Acid Modifications in rPA

Peptide measured[a]	EIC[b] (*m/z*)	Observed sequence[c]	GMP rPA ET[d] (min)	GMP rPA Amount[e] (peak area)	GMP rPA Fraction (%)[f] Native	GMP rPA Fraction (%)[f] Modified	GMP rPA P[g]	Treated rPA ET (min)	Treated rPA Amount (peak area)	Treated rPA Fraction (%) Native	Treated rPA Fraction (%) Modified	Treated rPA P
E398-K414 native	989–993	ENQLSQILAP**N**NYYPSK	33.9	86,572,612	97.6			34.0	59,906,612	96.0		
with D_{408}	989–993	ENQLSQILAP**D**NYYPSK	33.0	2,125,781		2.4	6th	32.9	2,499,021		4.0	6th
L450-R468 native	1086.5–1101	LDTDQVYGNIATYNFE**N**GR	33.6	312,576,950	86.4			33.7	200,097,441	79.3		
with $isoD_{466}$	1086.5–1101	LDTDQVYGNIATYNFE**isoD**GR	33.3	7,676,866		2.1		33.5	21,200,355		8.3	
with D_{466}	1086.5–1101	LDTDQVYGNIATYNFE**D**GR	34.0	25,535,047		7.1		34.0	21,260,297		8.5	
with Su_{466}	1086.5–1101	LDTDQVYGNIATYNFE**Su**GR	34.6	15,965,152		4.4		34.7	9,995,783		3.9	
I529-K545 native	947–951	IAFGFNEP**N**GNLQYQGK	32.4	369,916,899	64.5	13.6	3rd				20.7	3rd
with D_{537}	947–951	IAFGFNEP**D**GNLQYQGK	32.8	203,228,734		35.5	1st	32.4	53,714,472	14.8		
N601-K613 native	657–663	**NN**IAVGADESVVK	23.5	374,547,076	92.3			32.7	310,058,052		85.2	1st
with D_{601}	657–663	**D**NIAVGADESVVK	25.1	26,379,511		6.5	5th	23.5	266,491,781	91.7		
with D_{602}	657–663	N**D**IAVGADESVVK	24.4	4,851,556		1.2	7th	24.9	20,653,466		7.1	5th
E704-K722 native	705–713	ENTIINPSE**N**GDTST**N**GIKK	21.5	455,419,281	74.7			24.3	3,473,623		1.2	7th
with D_{713}	705–713	ENTIINPSE**D**GDTSTNGIKK	21.9	93,260,726		15.3		21.5	151,619,268	32.5		
with Su_{713}	705–713	ENTIINPSE**Su**GDTSTNGIKK	22.4	14,095,760		2.3		21.9	193,253,237		41.4	
with D_{719}	705–713	ENTIINPSENGDTST**D**GIKK	22.2	39,447,682		17.6	2nd	22.5	36,795,171		7.8	
with Su_{719}	705–713	ENTIINPSENGDTST**Su**GIKK	23.2	7,328,597		6.5		22.3	78,943,309		49.2	2nd
I505-K524 native	713–721	IAAVNPSDPLETTKPD**M**TLK	30.5	1,316,761,564	98.57	1.2		22.9	6,649,669		16.9	
with o521	713–721	IAAVNPSDPLETTKPD**o**TLK	27.8	19,163,804		7.7	4th				1.4	
						1.43		30.5	1,055,639,040	98.5	18.3	4th
								27.8	15,720,983		1.5	

[a]Tryptic peptides are designated by the numerical coordinates of the beginning and ending residues and indicate the state of modification for the sites under consideration. Standard single-letter nomenclature is used with the following changes: native, peptide contains expected amino acid sequence with no observed changes; D_{xxx}, peptide contains Asp at position xxx; $isoD_{xxx}$, peptide contains isoAsp at position xxx; Su_{xxx}, peptide contains succinimide at position xxx; o_{xxx}, measured peptide contains oxyMet at position xxx. Amino acid coordinates for rPA are as defined in Ref. 69.

[b]Extracted ion chromatograph (EIC) employed selected mass and tolerance settings for the peptide ion mass range indicated with precision of ± 0.2 *m/z*.

[c]Observed amino acid sequence of each tryptic peptide. Note that the KK miscleavage and triply charged ion product of peptide 704–722 was used for better measurement of two separate deamidations.

[d]Elution time of peptides separated by RP-HPLC prior to MS/MS collection and analysis, also = %B by virtue of the 5 min pregradient wash.

[e]Detection area (response *x* min) of indicated precursor ion as calculated using instrument default settings.

[f]Proportional amount of an observed peak area for each tryptic peptide carrying a site in *Native* form versus *Modified* form (D, isoD, Sum, or o) calculated as the ratio to the sum of areas for all observed peptide variants in that group.

[g]P, the percentile rank order of deamidation among all measured Asn sites.

DOI 10.1002/prot

Robinson algorithm [Fig. 10(A)]. In this regard, Zomber et al.[63] recently reported tantalizing MALDI-TOF-MS fingerprinting data for PA that concur with and differ from our findings of Asp deamidation, first reported earlier and fully described here. In agreement, deamidation at N713 and N719 were inferred as the cause of a +2 Da shift of peptide 704–723 which contains four Asn residues that could possibly degrade. However, without MS/MS sequencing, individual levels of deamidation and direct proof of which Asn had actually modified could not be ascertained directly on digested protein, but instead was deduced from theoretical predictions of deamidation and from measures of model synthetic peptides.[38] Aged synthetic peptides were reported to exhibit 100% deamidation at these two sites,[63] where we found no more than 37% deamidation at either of these sites in treated PA protein of high isoform content (Table I, Figs. 5 and 6). Also in concordance with data reported here, no evidence was found for deamidation at N10 or N306, which is in sharp contrast to predictions from the Robinson algorithm that calculates both of these sites to be among the most reactive Asn residues in PA (Fig. 10). Our findings are also comparable with respect to possible deamidation at N162, a site of possible significance as it juxtaposes the furin cleavage site. Namely, neither approach found unequivocal evidence of deamidation at this position within fresh PA protein. Using aged isolates of cleaved and isolated PA_{20}, an observed +1 Da mass shift for peptide 149–167 was attributed entirely to one (N162) of two Asn residues present on the peptide, based on theoretical rates of deamidation.[63] Instead, inhibition of furin activity was demonstrated by substitutions analogous to position N162 of synthetic peptide mimetics.[63] We found no convincing evidence of modification at N162 even in aged PA_{83} protein (Fig. 7), and therefore propose that the observed inhibition of furin activity for degraded PA protein may be due to significant deamidation at other positions, as described below. Thus, findings reported previously and herein reflect two areas of agreement. First, that the specific locations of multiple deamidation and their individual contributions to an observed mass shift in a protein cannot be directly and unequivocally determined for proteolyzed protein using MALDI-TOF-MS fingerprinting profiles alone. We show instead that such determination could be directly achieved by LC (i.e., nonmass-based) peptide separation before MS analysis with concurrent MS/MS sequence analysis. Second, that the Robinson algorithm for predicting deamidation does not fit experimental data for at least two Asn residues in PA protein (N10, N306), and our own findings indicate that deamidation at several other Asn residues also do not conform to predictions, as discussed further below.

We note two aspects of this method that are not fully optimized and may generate inaccuracy in measurement of deamidation depending on the particular peptide being inspected. First, over estimation of natural deamidation may arise from conditions of treatment *in vitro* that can enhance deamidation including proteolysis.[66] However, unlike other published work,[66] these proteolysis procedures did not expose samples to denaturation, cysteine reduction, or alkylation. The necessary reactants (chaotrope, reducing agent, alkylating agent) have high dielectric constants which is one factor known to enhance Asp deamidation *in vitro*. Chemical environments of high pH, high ionic strength, or high dielectric field strength stabilize the protonated state of the attacking peptide bond nitrogen, which is the nucleophilic anion that initiates formation of the succinimide intermediate and rate-limiting step of Asp deamidation (see Fig. 1).[77,78] Variable increases in deamidation were observed for test samples comparing treatments of 4 h versus the standard 18 h (data not shown). Nonetheless, induced amounts would cancel one another upon calculating changes in deamidation since all proteolysis reactions used identical solvent, temperature, and duration. Secondly, under representation of natural deamidation may arise from unaccounted forms of deamidation, specifically the isoAsp end product and the succinimide intermediate. We observed these forms only in three residues of rPA (N466, N713, and N719). Yet formation of these components is variable and unpredictable, and their observation by RP-HPLC can be strongly dependent on amino acid sequence which differs between distinct peptides. Indeed, their irregular appearance is neither unexpected nor unprecedented,[66] and similar errors afflict many MS measurements of protein deamidation. Alternatively, direct and definitive assignment of deamidation and isoAsp content can be achieved using instruments of high-mass accuracy.[60,62,79] Supportive evidence for deamidation and isoaspartate at these sites has been observed by electron capture dissociation on an FTMS instrument (P. O'Connor, unpublished data), as will be described separately.

Analysis of Gel-Isolated rPA Isoforms: Percent Deamidation Associates With Isoform Net Negative Charge and Isoform Complexity

Next, we studied purified isoforms to look for evidence that might support the supposed correlation between site specific deamidation and an individual isoform or pattern of isoforms. This cannot be evaluated using purified rPA protein because such samples are demonstrably heterogenous, and a measurement of deamidation in fact represents a population average of all individual isoforms present in the analyzed sample. Therefore, isolated protein isoforms were excised from native PhastGel bands and from 2-DE gel spots then analyzed for their individual levels of deamidation. As in prior findings using averaged measurement of unfractionated protein, Asn N537 showed the highest level of measured deamidation in nearly every isolated charge isoform (Figs. 3 and 4). Although the absolute amount of peptide 529–545 varied due to differing protein concentration in each isoform band, the percent deamidation at N537 clearly increased with increasing molecular net negative charge of isoform species. This trend was evident among isoform

bands separated by native PAGE (Fig. 3, hatched box) and isoform spots separated by 2-DE (Fig. 4, hatched boxes). Some bands/spots contained too little protein for confident measurement (Fig. 3, bands 1 & 5; Fig. 4, spots at extreme pI values), but most forms generally reflected the trend of increasing percent deamidation with increasing negative charge. All observed gel isoforms contained some amount of deamidation at position N537, and the few cases of complete deamidation occurred in isoforms of extreme mobility or limiting concentration [e.g., Fig. 3, band 5; Fig. 4(A), spots 1–3]. Minor isoforms that were less acidic than the major isoforms also contained lower percentage deamidation at residue N537 [Figs. 3, bands 1 and 2; 4(A), spot 6; 4(B), spot 8; 4(C), spots 5 and 6; 4(D), spots 7–8; 4(E), spots 6 and 7; 4(F), spot 8]. These data show that mean Asn deamidation, as dominated by N537, clearly increased with increasing molecule acidity. These findings were the first evidence to directly associate site-specific Asn deamidation charge heterogeneity in PA, as was released in part previously. These data also concur with our postulate that the native, unmodified form of PA is not the isoform of greatest abundance.

Thus, two (N537 and N713) of seven Asn residues observed to deamidate in PA protein varied noticeably in association with isoform content, increasing directly with acidity and isoform complexity as separated by native PAGE and 2-DE (Figs. 3–6). A similar but less apparent trend was observed at four of the remaining five Asn residues, as seen individually and reflected in the mean total deamidation (Figs. 5 and 6). Despite these congruencies, no single deamidation event or combination thereof was uniquely associated with any single isoform spot, band, or pattern-whether inspected for the presence, absence, or change in percent deamidation. Each charge-separated isoform is itself heterogeneous in deamidation content. Indeed, since each separable PA isoform simultaneously contains several sites of Asn deamidation that are nonidentical amongst themselves or between isoforms, these data clearly disprove the early hypothesis that proposed one deamidation per isoform band for native PA protein. A reasonable explanation to account for these data is to propose that each visible isoform comprises a distinct charge class of molecules representing a distinct number of deamidations irrespective of their individual locations. A similar conclusion was drawn in the past on other deamidated proteins, a recent example being the study of deamidation in human plasma blood proteins.[80]

We note that isoform complexity was not observed to be identical among the three methods of fractionation, as might otherwise be supposed for a universal explanation. However, PA protein experienced different physical conditions during these methods of separation. Samples were fully denatured during the first step of fractionation in 2-DE, but remained folded during fractionation by native PAGE and CEIF and were therefore likely to be partially ionized or shielded. If all substantial 2-DE isoforms and residues of significant deamidation were accounted for by these data, then the simplest explanation for this observed isoform complexity is that 2-DE provided the greatest observed degree of fractionation, and that eight differentially charged isoform spots of PA resulted from seven observed deamidations, in agreement with charge states caused by variable deamidation at seven Asn residues plus a native form. Fractionation of PA by native PAGE and CEIF provided less fractionation and thus fewer visible isoforms. This establishes, for the first time, that charge isoforms of PA are associated with the presence of fractional deamidation at seven Asn residues, and that deamidation at one of these sites (N537) varies in direct proportion with isoform charge. That position N537, and not the predicted residue N713, had the highest observed deamidation in PA impacts the utility of *in silico* predictions for PA deamidation and the possible development of specific assays of rPA stability, as later discussed.

Site-Specific Asn deamidation increases with protein purity and aging

Throughout this study, isoform complexity and measured Asn deamidation slowly increased as separate experiments were performed on the same frozen aliquot of pure rPA protein. Because patterns and percent deamidation began to change more substantially than that observed for some R & D lots held frozen at −70°C since early development (ca. 17 years), we suspected the apparent aging was caused by sequential freeze/thaw/hold cycles of the same aliquot while being repeatedly accessed over time. This effect was reproduced upon intentional sequential freeze/thaw/hold treatment of a fresh lot of GMP rPA protein for which all affected sites increased in modification. To test for a correlation between levels of deamidation and gross apparent PA protein degradation, as indicated by isoform complexity, we measured each of the confirmed sites on freshly thawed GMP rPA versus the same lot of protein treated by repeated freeze/thaw/hold to achieve accelerated aging. Percentage modification increased and percentile rank order did not change after treatment [Table I, Fig. 10(A)], except for N602 which remained very low. Isoform spots at extreme pH or low concentration also did not fit the trend. Archived lots of R & D preparations showed similar rank order of deamidation, and isoform complexity appeared to vary proportionally with the mean percent deamidation averaged across all measured sites (Fig. 6). As seen before, the strongest association was apparent for the two most highly deamidated sites, N537 and N713. Notwithstanding measurements near the limit of detection, the overall association between measured deamidation and isoform complexity was clearly evident in both fresh and aged protein, whether considered individually or together as an average [Figs. 4, (insets for B, D, F), 5, 6, 8, Table I]. This mirrored a similar general trend for loss of protein biological activity described below.

One tryptic peptide required additional analysis to calculate percent deamidation. Peptide 704–722 contained

two sites of deamidation (N713, N719) and theoretically could have contained double deamidation on a single peptide. We cannot exclude the possibility that such a peptide may be present at very low levels. Although four isoform peptide peaks for such precursor ions were observed, they overlapped substantially and their EIC peak areas were very small and nearly immeasurable using doubly charged ions. In contrast, triply charged precursor ions yielded substantially more intense and measurable peak areas, and were instead used for calculating deamidation levels (Materials and Methods, Table I). Moreover, the detection, confirmation, and use of succinimide intermediates assisted measurements since the delta mass of −17 circumvented confusion otherwise caused by overlapping heavy isotopes and the delta mass of +1 for deamidation. In contrast, peptide 601–613 also contained two deamidated Asn (N601, N602) but three forms were well separated by RP-HPLC. Here, differing amino acid sequences likely had a large impact on the fractionation and discrimination of smaller peptides. The absence of simultaneous, tandem Asn deamidation at N601 and N602 concurs with the Robinson algorithm which calculates very low deamidation for any such an arrangement.[60] As discussed below, most of the rates inferred from measured deamidation in rPA did not concur with predicted relative order.

In summary, Asn deamidation generally increased in association with rPA isoform complexity, and the method reported here will enable global inspection of site-specific deamidation in PA as a function of many treatments. The findings reported here also complicate the goal of reaching a precise atomic description of rPA protein isoform content and its relationship to rPA product stability by dispelling earlier notions of a proposed direct correspondence between site specific deamidation and isoform identity. At present, we showed that total molecular deamidation plainly correlated with total net negative charge and isoform complexity, but the precise combinations of site-specific deamidation among the different Asn residues and visible isoforms remains undefined. In contrast, the loss of rPA biological activity was observed to correlate with increased deamidation as shown next.

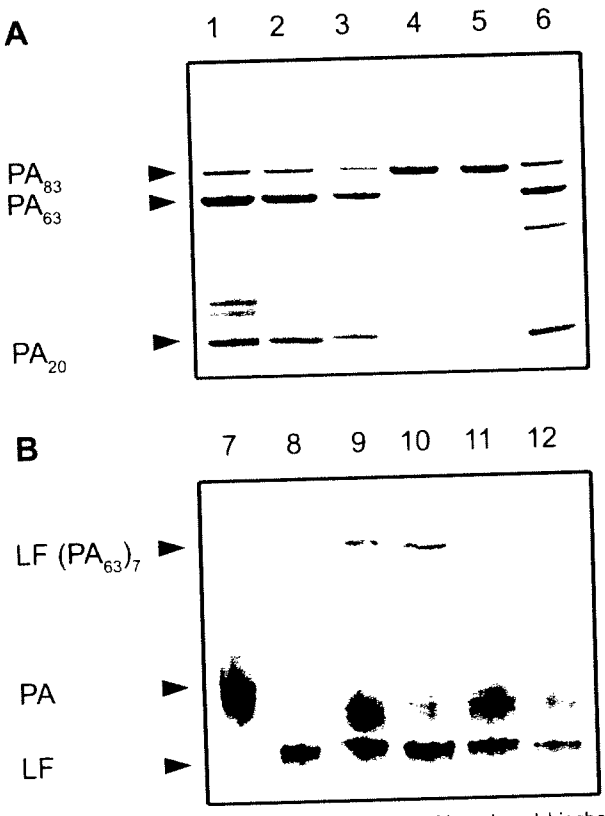

Fig. 9. Asparagine deamidation associates with reduced biochemical activities of PA. (**A**) gel shift assay for furin-cleavage activity. (**B**) gel shift assay for holoenzyme-formation activity. Lot identities, mean deamidation of rPA (in parentheses) and sample content per lane as follows: 1, List Biologicals PA (10.5%); 2, GMP rPA (12.2%); 3, 1996 pool A rPA (18.2%); 4, 1996 pool B rPA (26.5%); 5, 1995 rPA (27.2%); 6, aged GMP rPA (26.5%); 7, GMP rPA; 8, LF; 9, LF + GMP rPA; 10, LF +1996 pool A rPA; 11, LF +1996 pool B rPA; 12, LF + aged GMP rPA. Both assays performed as described previously.[23]

Analysis of Biochemical Activities: Asn Deamidation Associates With Loss of Furin Cleavage and Holotoxin Assembly

Three interrelated biochemical activities of rPA were measured using gel-shift assays to investigate a possible effect by deamidation on protein activity. As reported previously,[21] these assays test the combined functions of site-specific proteolysis by furin to generate PA_{63}, intermolecular protein associations that create the heptameric $(PA_{63})_7$ form, and then binding of LF to create the $LF(PA_{63})_7$ holoenzyme. Modification across all seven Asn sites at a mean total deamidation ranging from 10.5% (List rPA) to 18.2% (rPA lot a, 1996 pool A) did not visibly affect furin cleavage, heptamerization, or holoenzyme formation [Fig. 9(A and B), lanes 2, 3, 9, 10, and legend]. On the other hand, full inhibitions of these activities occured at 26.5% mean total deamidation [Fig. 9(A and B), lanes 4 and 11]. While artificially aged GMP protein containing 26% mean total deamidation retained partial cleavage activity, it did not retain activity for holoenzyme formation (Fig. 9, lane 12). Although residues N713, N537, and N719 had the greatest incremental increase in deamidation between fresh and aged protein [Fig. 10(A), % change], the apparent correlation cannot be statistically evaluated and therefore we cannot yet propose whether deamidation at these sites exerts a primary causative impact on loss of biochemical function.

Thus, we found that the biochemical and biophysical activities of PA were sensitive to Asn deamidation. The ability of rPA to function as substrate for site-specific cleavage, to participate in heptamerization, and then bind LF to form holoenzyme complex were inhibited above a threshold level of 26% mean total deamidation across the seven described residues. Although deamidation varied among individual sites, and increased differentially by artificial aging, their pattern of deamidation

A

Asn Site	$t_{1/2}$ (1,000 days)	Rank Order			Change	
		P	F	T	%	Rank
713	0.024	1st	2nd	2nd	180	1st
162	0.038	2nd	-	-	-	
719	0.049	3rd	4th	4th	138	3rd
306	0.053	4th	-	-	-	
010	0.057	5th	-	-	-	
102	0.067	6th	-	-	-	
006	0.081	7th	-	-	-	
281	0.117	8th	-	-	-	
466	0.133	9th	3rd	3rd	52	5th
537	0.219	10th	1st	1st	140	2nd
408	4.363	37th	6th	6th	67	4th
601	48.15	57th	5th	5th	9	6th
602	2,594	68th	7th	7th	0	-

B

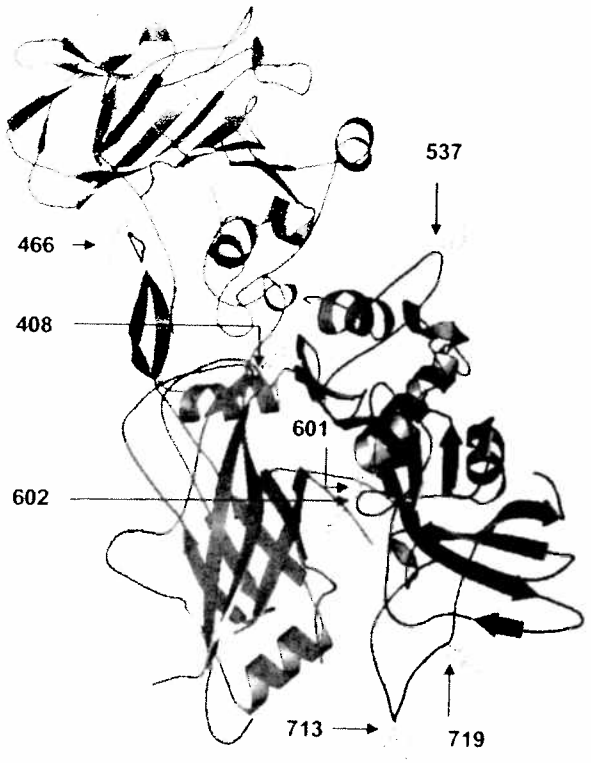

Fig. 10. Comparison of computational and observed deamidation in rPA. (**A**) Table comparing rank order of observed Asn deamidation to that predicted by rate at www.deamidation.org using the protein database identifier for PA (1ACC). Abbreviations as follows: Asn site, amino acid coordinate of Asn as defined in Figure 2. $t_{1/2}$, half life in days of deamidation calculated from the theoretical coefficient of deamidation; rank order for propensity of deamidation as listed by: *P*, predicted rate calculated by the Robinson algorithm; *F*, observed percentage for fresh PA protein; *T*, observed percentage for treated PA protein; 0, no deamidation observed; (**B**) Projection of seven observed sites of deamidation onto the three-dimensional structure of PA. Arrows mark deamidated Asp with numeric designation by coordinate number, as defined in Figure 5; pink dots, projection of original asparginyl side group. Color scheme as follows: domain 1 (orange, residues 1–258) contains two calcium-binding sites, the cleavage site for furin class proteases, and the binding site for EF and lethal LF. Domain 2 (red, 259–487) forms most of the channel and protein–protein interactions. Domain 3 (green, 488–595) may play a role in oligomerization. Domain 4 (blue, 596–735) is responsible for binding the cell-surface receptor; (**C**; following page), Projection of seven observed Asn deamidation sites onto a space-filling model of the X-ray structure of monomeric PA, and rotated 180° around its long axis for full viewing. Color scheme as for panel B except domain 1 is pink.; (**D**) Projection of seven observed Asn deamidation sites onto the modeled structure of PA heptameric prepore $(PA_{63})_7$, central pore axis angled slightly down and left, and one LF-binding domain (pink) removed (dotted trapezoid), to expose buried sites and position others for viewing. Deamidation at residue N537 is highest among all samples tested, while deamidation at residues N408 and N466 statistically correlate with loss of PA biological activity. Same coloration as in panel C except LF/EF factor binding sites are shown in orange.

does not yet allow the assignment of a direct causal relationship between the loss of biochemical activity and modification at any single site. Site-directed mutagenesis to change individual sites to Asp may help to elucidate a specific cause for loss of structural activity.

Analysis of Biological Activity: Cytotoxic Activity Correlates Inversely With Isoform Complexity and Asn Deamidation

We also employed $LF(rPA_{63})_7$ holoenzyme, formed in the same manner, to test cytotoxicity as an indicator of the effect of deamidation on rPA biological activity. This assay is believed to test the ability of PA to translocate LF across the cell membrane which then kills macrophage cells. The dose of protein causing 50% killing (ED_{50}) was measured, as standardized across experiments by comparison to fully active PA. For GMP grade rPA and R & D lots of rPA, both ED_{50} and site-specific deamidation generally increased with increasing isoform complexity (Figs. 5 and 6). Comparing mean total deamidation across all seven measured sites to ED_{50} values showed a statistical correlation between deamidation and loss of biological activity ($r = 0.96144$, $P = 0.0386$) considering the four lots shown in Figure 6. Statistically significant correlation between the loss of biological activity and changes in individual Asn deamidation were observed as follows: N408, $r = 0.99473$, $P = 0.0053$; N466, $r = 0.97894$, $P = 0.0211$; N601, $r = 0.95546$, $P = 0.0445$. Interestingly, deamidation in the most reactive position, N537, did not vary statistically with loss of biological activity ($r = 0.88351$, $P = 0.1165$). Also, although

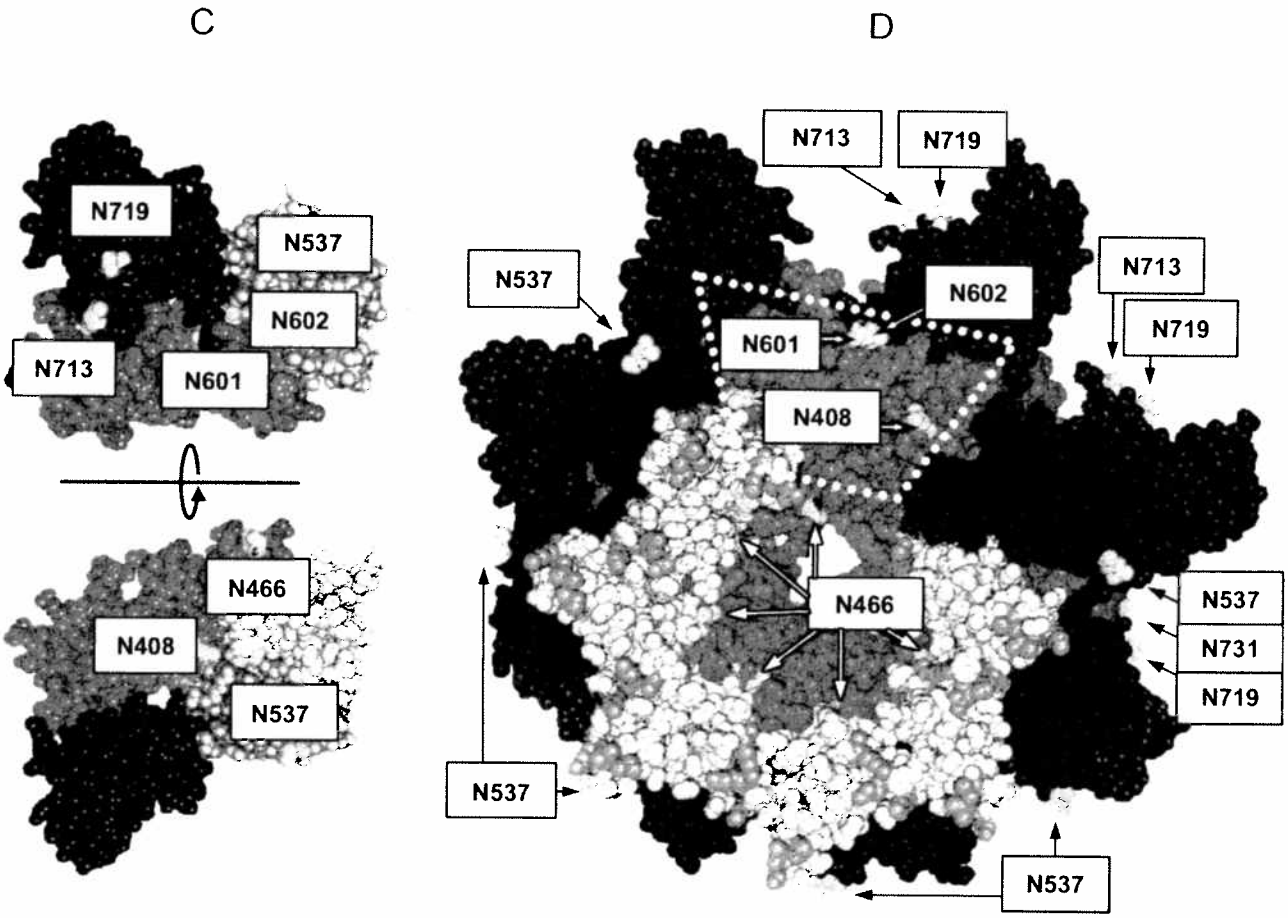

Figure 10. (Continued.)

deamidation at the second most deamidated residue, N713, appeared to vary directly with loss of biological activity, statistical parameters ($r = 0.94365$, $P = 0.0563$) fell just outside levels of significance and therefore a definitive association was not supported. Of the remaining sites lacking statistical relationship in this regard, one showed moderate deamidation (N719) and the other showed the lowest measured level of deamidation (N602) and did not change. Among these data, only deamidation levels at N408, N466, and N601 varied directly and significantly with the loss of rPA cytotoxic activity.

Thus, we found no supportive evidence of deamidation in rPA protein at position N162 which juxtaposes the furin cleavage site,[63] but these data indicated that inhibition of cleavage correlated with deamidation elsewhere. In spite of the high deamidation at N537, and accelerated deamidation at N713 and N719 caused by freeze/thaw/hold treatment, variation in none of these residues correlated statistically with loss of biological activity. Instead, the loss of activity appeared to be associated with one or more deamidations at positions N408, N466, and N601 since these did vary with statistical significance upon loss of biological activity. It is reasonable that the sites of slowest observed degradation exerted the greatest effect on biological activity and vice versa, otherwise selective pressure would have generated different structure/function relationships to maintain anthrax holotoxin that degrades naturally while retaining biological function *in vivo*. This hypothesis may be testable using site-directed substitutions in whole PA protein.

With regard to eliciting protective immunity as a vaccine antigen, we note that although both of the major isoforms provide equivalent protection against lethal anthrax challenge as compared to the whole pharmaceutical preparation,[23,70] we now know that neither of these primary isoforms represented native (unmodified) protein: both contained various amounts of deamidation at the seven labile positions described herein. These findings demonstrate that certain specific deamidations present in the test article did not negatively impact its measurable efficacy as a vaccine substance or in PA-mediated biological activity *in vitro*. While the state of protein modification *in vivo* during disease has not been reported, PA is likely to degrade at these residues based on our findings that rPA deamidates rapidly in *B. anthracis* during expression. Thus, the biological activity of rPA is apparently tolerant to a range of Asn deamida-

tions including, most notably, 35% and 85% deamidation at position N537 within its two predominant isoforms.

Measured Asn Deamidation Differs From Theoretical Predictions for PA

From the very first confirmation of site-specific deamidation in this study, we observed that the apparent rates of deamidation in rPA did not concur with theoretical predictions calculated by the method of Robinson and Robinson.[60,81] The relative rates of deamidation, as inferred in this study from the rank order of observed percent deamidation, align with only two theoretical predictions [Fig. 10(A)]. Surprisingly, N537 is the most deamidated site we measured in PA, even though it is predicted to be tenth in rank order position of reactivity as calculated by the algorithm [Fig. 10(A), columns "*P*" vs. "*F*"]. After accounting for N537 at 1st place for cumulative percent deamidation, only N713 and N719 aligned in comparative ordinal position with their predicted activities. Additionally, residues occupying the calculated rank positions of 4th through 8th were in fact not observed to be deamidated at all, while three sites predicted to be very poorly reactive (N408, N601, and N602) instead showed measurable deamidation. All of these deamidations increased with protein degradation within the same rank order for cumulative deamidation [Fig. 10(A), columns "*F*" vs. "*T*"]. However, by comparing the incremental change in deamidation between fresh and treated protein as an approximate gauge for the rate of deamidation, residue N713 appears to show the highest reactivity *in vitro* in concordance with the Robinson algorithm [Table I, Fig. 10(A), % rank change]. By this measure, residue N719 also concurs in ordinal rank with predicted rates. Residues N601, N602, and N408 show the lowest rate of deamidation upon treatment, which concurs with the Robinson algorithm that predicts very poor reactivity for residues followed by Ile or Asn. Also in general agreement with model predictions, the sites of highest measured deamidation (N537, N713, N466, N719) have a C-terminal Gly, a neighboring residue predicted to best enable deamidation.[60,81] The three most deamidated of these residues (N537, N713, N466) appear to be situated at tight bends and be solvent exposed in the monomer [Fig. 10(A)], factors that may facilitate deamidation. Aside from these few agreements, most Asn did not deamidate as predicted. We suggest these data may indicate two classes of deamidation, that which occurs *in vitro* and appears to cause deamidation somewhat approximating predicted rates, as in N713 and N719 after accelerated aging, and deamidation that occurs *in vivo* before protein purification and creates unpredicted levels of deamidation, as reflected in N537, N466, N408, and N601. The specific incongruence between actual and predicted deamidation behavior for PA protein may conceivably have been due to differing buffer conditions which are known to strongly affect the rates of spontaneous deamidation,[38] but also introduce a question of whether other factor(s) may affect deamidation of PA *in vivo*, particularly with respect to N537. A description of specific enzymatic deamidation or even a possible functional role for deamidation in PA activity remains to be discovered. From these data we deduced that, at least for the PA protein produced in *B. anthracis* and purified by the methods described, model calculations of deamidation do not accurately predict the actual net levels of deamidation for many its 68 asparagine residues.

Mapping Observed Asn Deamidations onto the Known Spatial Structure of PA Monomer and Heptamer

To explore the possible effects of observed deamidation on PA protein structure and function, these seven positions of deamidation were mapped onto the X-ray structures of monomeric PA (PDB code 1ACC) and PA heptameric prepore (ITZO).[82,83] The positional substitutions were then evaluated with respect to known functional and structural domains and interprotein contacts,[14,84,85–87] considering first the four residues (N408, N466, N601, N713) which have the greatest measured impact on biological activity of PA protein (Figs. 5 and 6). Two of these, N408 and N466, lie in domain 2, and show the highest observed correlation between deamidation and loss of PA biological activity as conveyed through LF cytotoxicity. This region is involved in heptamerization and also contains the insertion loop which forms the lumen of the PA pore. Residue N408 is situated nearest to K496 of domain 3, and may possibly be close enough to form a salt bridge in the deamidated state (i.e., as D408). Although in close proximity to I316 of a neighboring PA monomer, N408 is buried in the heptameric prepore structure and adjoins domain 1′ which binds EF and LF effector proteins [dashed trapezoid in Fig. 10(D)]. This residue also comprises the apex of a short beta bend (409 – 411). This local structure may explain why the usual inhibitory effects on deamidation by a C-terminal Asn were less prominent for N408. Residue N466 is also situated near the factor binding regions of domain 1′ but located at the top of the pore lumen in the heptameric structure [Fig. 10(D)]. Its closest spatial neighbors are the side groups of N463 and R468, plus R470 in domain 2 of the same PA monomer. The next closest are W226 and S230 in domain 1′ in the next subunit clockwise. Although none of these residues form part of the known EF/LF binding patch,[88] this region may be close enough [Fig. 10(D)] for deamidation to exert an effect through altered charge or disruption of protein folding. In the holoenzyme structure, deamidation at N466 replaces a normal positive dipole moment and hydrogen donor with a full negative charge and hydrogen acceptor, therein creating a substantially new localized environment comprising a seven position ring within the pore lumen. Such change may conceivably impact the tight passage of effector proteins through the PA pore.

Four of the remaining modified sites (N601, N602, N713, and N719) are located within domain 4, and the

final site (N537) is situated in domain 3 [Fig. 10(A)]. Residues N601 and N602 are at the beginning of domain 4, buried within the heptamer molecule, and contact domains 2 and 3 of the same PA monomer subunit. Residues 713 and N719 are exposed on outer side of domain 4 and flank the ATR binding site at 714–719.[83] A structural rationale for why deamidation at N601 correlates strongly with loss of biological activity was not immediately apparent. Residue N537, the most highly deamidated Asn of PA, appears also to be the most exposed and exterior Asn in the modeled structures [Fig. 10(D)]. Its positioning at the apex of a solvent-exposed outer loop [Fig. 10(A)] may also support its high tendency to deamidate. The peripheral location of this residue in the heptamer, away from ATR or effector binding regions, also concurs with the absence of a prominent effect by N537 deamidation on the biochemical, biological, and immunological activity of rPA.

CONCLUSIONS

We draw the following conclusions from this study of structural heterogeneity in rPA. Micro-charge heterogeneity of the PA protein is caused by partial and dissimilar deamidation across at least seven asparagine residues: N408, N466, N537, N601, N602, N713, and N719. For freshly thawed pharmaceutical grade rPA, these deamidations are the only observed post-translational modifications capable of imparting additional charge to the protein, and no other amino acid modification is present except for a minute amount of methonine oxidation (M521). Position N537 has the highest cumulative level of deamidation in GMP grade rPA protein, commercial PA protein, research and development grade protein, as well as in purified rPA isoforms, and remains the highest-ranking modified position after intentional degradation by freeze/thaw/hold treatment. Neither of the two predominant isoforms present in GMP-grade and commercial grade PA has a molecular charge corresponding to native protein, and both of these isoforms are partially deamidated across all seven of the labile Asn. No specific site of deamidation can yet be attributed to the appearance of a specific isoform band, spot, peak, or pattern. By inspection of isoform patterning, and by inference from measured modifications on fresh and aged protein, rPA appears to be rapidly deamidated *in vivo* and then deamidates to a smaller incremental degree *in vitro*. Mean percent deamidation increases in direct proportion with isoform complexity. After intentional degradation by freeze/thaw/hold treatment, the rank order of percent deamidation among these seven residues does not change, but the apparent rates of deamidation for N713 and N719 trends toward their predicted rates. Whether measured in freshly thawed or treated protein, most of these deamidations do not concur with their theoretical ordinal rank of deamidation. The Robinson algorithm for predicting deamidation at Asn and Gln residues in protein is presently not well suited for preselecting specific residues with which to assay rPA structure or stability. Isoform complexity and asparagine deamidation associates inversely with PA biochemical and biological activity at four residues: N408, N466, N601, and N713. Deamidation at N408 and N466 show the strongest statistical correlation with the loss of PA biological activity *in vitro*. Thus, with respect to measuring PA degradation by deamidation, N537 is a suitable biomarker for general structural stability, while N408 and N466 are better suited for assays of biological stability. The high level of deamidation at N537 in all isoforms and lack of apparent effect on biochemical or biological activity concurs with findings from our prior study which demonstrated that the two primary isoforms of rPA are equally protective as vaccine immunogens against lethal anthrax exposure.[23,70] Finally, the method described herein for collecting and analyzing spectral data is generally applicable for the study of deamidation in other proteins because it employs an LC-ESI-MS/MS instrument of nominal mass accuracy and because calculations are performed strictly from direct empirical measurements without dependence on theoretical models.

ACKNOWLEDGMENTS

We thank R. Cushman for laboratory assistance, S. Norris for statistical analysis, C. Beardsley for instrument care, C. Haney, J. Roark, D. Horn, and B. Davis for instrument and software technical support, B. Hood and T. Veenstra for early conversations, and L. Ostby for preparation of illustrations. We are grateful to Jason J. Cournoyer and Peter B. O'Connor for testing some of these deamidation sites by electron capture dissociation FTMS, and to P. O'Connor and T. Nguyen for critical review of the manuscript.

REFERENCES

1. Friedlander AM, Pittman PR, Parker GW. Anthrax vaccine: evidence for safety and efficacy against inhalational anthrax. JAMA 1999;282:2104–2106.
2. Friedlander AM, Welkos SL, Ivins BE. Anthrax vaccines. Curr Top Microbiol Immunol 2002;271:33–60.
3. Ivins BE, Pitt ML, Fellows PF, Farchaus JW, Benner GE, Waag DM, Little SF, Anderson GW, Jr, Gibbs PH, Friedlander AM. Comparative efficacy of experimental anthrax vaccine candidates against inhalation anthrax in rhesus macaques. Vaccine 1998;16(11/12):1141–1148.
4. Leppla S. Production and purification of anthrax toxin. In: Harshman S, editor. Methods in Enzymology, Vol. 165. Orlando, FL: Academic Press; 1988. pp 103–116.
5. Duesbery NS, Webb CP, Leppla SH, Gordon VM, Klimpel KR, Copeland TD, Ahn NG, Oskarsson MK, Fukasawa K, Paull KD, Vande Woude GF. Proteolytic inactivation of MAP-kinase-kinase by anthrax lethal factor. Science 1998;280:734–737.
6. Leppla SH. Anthrax toxin edema factor: a bacterial adenylate cyclase that increases cyclic AMP concentrations of eukaryotic cells. Proc Natl Acad Sci USA 1982;79:3162–3166.
7. Pellizzari R, Guidi-Rontani C, Vitale G, Mock M, Montecucco C. Lethal factor of Bacillus anthracis cleaves the N-terminus of MAPKKs: analysis of the intracellular consequences in macrophages. Int J Med Microbiol 2000;290(4/5):421–427.
8. Vitale G, Bernardi L, Napolitani G, Mock M, Montecucco C. Susceptibility of mitogen-activated protein kinase kinase family members to proteolysis by anthrax lethal factor. Biochem J 2000;352(Part 3):739–745.

9. Friedlander AM. Clinical aspects, diagnosis and treatment of anthrax. J Appl Microbiol 1999;87:303.
10. Bradley KA, Mogridge J, Mourez M, Collier RJ, Young JA. Identification of the cellular receptor for anthrax toxin. Nature 2001;414:225–229.
11. Klimpel KR, Molloy SS, Thomas G, Leppla SH. Anthrax toxin protective antigen is activated by a cell surface protease with the sequence specificity and catalytic properties of furin. Proc Natl Acad Sci USA 1992;89:10277–10281.
12. Singh Y, Chaudhary VK, Leppla SH. A deleted variant of *Bacillus anthracis* protective antigen is non-toxic and blocks anthrax toxin action in vivo. J Biol Chem 1989;264:19103–19107.
13. Christensen KA, Krantz BA, Collier RJ. Assembly and disassembly kinetics of anthrax toxin complexes. Biochemistry 2006; 45:2380–2386.
14. Mogridge J, Cunningham K, Collier RJ. Stoichiometry of anthrax toxin complexes. Biochemistry 2002;41:1079–1082.
15. Miller CJ, Elliott JL, Collier RJ. Anthrax protective antigen: prepore-to-pore conversion. Biochemistry 1999;38:10432–10441.
16. Abrami L, Lindsay M, Parton RG, Leppla SH, van der Goot FG. Membrane insertion of anthrax protective antigen and cytoplasmic delivery of lethal factor occur at different stages of the endocytic pathway. J Cell Biol 2004;166:645–651.
17. Qa'dan M, Christensen KA, Zhang L, Roberts TM, Collier RJ. Membrane insertion by anthrax protective antigen in cultured cells. Mol Cell Biol 2005;25:5492–5498.
18. Nguyen TL. Three-dimensional model of the pore form of anthrax protective antigen. Structure and biological implications. J Biomol Struct Dyn 2004;22(3):253–265.
19. Duesbery NS, Vande Woude GF. Anthrax toxins. Cell Mol Life Sci 1999;55:1599–1609.
20. Vitale G, Pellizzari R, Recchi C, Napolitani G, Mock M, Montecucco C. Anthrax lethal factor cleaves the N-terminus of MAPKKS and induces tyrosine/threonine phosphorylation of MAPKS in cultured macrophages. J Appl Microbiol 1999;87:288.
21. Panchal RG, Halverson KM, Ribot W, Lane D, Kenny T, Abshire TG, Ezzell JW, Hoover TA, Powell B, Little S, Kasianowicz JJ, Bavari S. Purified *Bacillus anthracis* lethal toxin complex formed in vitro and during infection exhibits functional and biological activity. J Biol Chem 2005;280:10834–10839.
22. Turnbull PC. Anthrax vaccines: past, present and future. Vaccine 1991;9:533–539.
23. Ribot WJ, Powell BS, Ivins BE, Little SF, Johnson WM, Hoover TA, Norris SL, Adamovicz JJ, Friedlander AM, Andrews GP. Comparative vaccine efficacy of different isoforms of recombinant protective antigen against *Bacillus anthracis* spore challenge in rabbits. Vaccine 2006;24:3469–3476.
24. Jendrek S, Little SF, Hem S, Mitra G, Giardina S. Evaluation of the compatibility of a second generation recombinant anthrax vaccine with aluminum-containing adjuvants. Vaccine 2003; 21(21/22):3011–3018.
25. Whiting GC, Rijpkema S, Adams T, Corbel MJ. Characterisation of adsorbed anthrax vaccine by two-dimensional gel electrophoresis. Vaccine 2004;22(31/32):4245–4251.
26. Turnbull PC. Introduction: anthrax history, disease and ecology. Curr Top Microbiol Immunol 2002;271:1–19.
27. Little SF, Webster WM, Ivins BE, Fellows PF, Norris SL, Andrews GP. Development of an in vitro-based potency assay for anthrax vaccine. Vaccine 2004;22(21/22):2843–2852.
28. Pitt ML, Little SF, Ivins BE, Fellows P, Barth J, Hewetson J, Gibbs P, Dertzbaugh M, Friedlander AM. In vitro correlate of immunity in a rabbit model of inhalational anthrax. Vaccine 2001;19:4768–4773.
29. Department of Health and Human Services, Food and Drug Administration. 21 CFR Parts 201 and 610, Docket no. 1980N-0208. Biological products: bacterial vaccines and toxoids, Implementation of efficacy review, Vol. 29, no. 249. Federal register, December 29, 2004. Available at http://www.fda.gov/ohrms/dockets/98fr/04-28322.htm
30. Federal register vol. 67, no. 105, May 31, 2002. 21 CFR Parts 314 and 601, Docket no. 98N-0237. New drug and biological products, Evidence needed to demonstrate effectiveness of new drugs when human efficacy studies are not ethical or feasible. Available at http://www.fda.gov/cber/rules/humeffic.pdf
31. Manning MC, Patel K, Borchardt RT. Stability of protein pharmaceuticals. Pharm Res 1989;6:903–918.
32. Cleland JL, Powell MF, Shire SJ. The development of stable protein formulations: a close look at protein aggregation, deamidation, and oxidation. Crit Rev Ther Drug Carrier Syst 1993;10: 307–377.
33. Geiger T, Clarke S. Deamidation, isomerization, and racemization at asparaginyl and aspartyl residues in peptides. Succinimide-linked reactions that contribute to protein degradation. J Biol Chem 1987;262:785–794.
34. Clarke S. Propensity for spontaneous succinimide formation from aspartyl and asparaginyl residues in cellular proteins. Int J Pept Protein Res 1987;30:808–821.
35. Stephenson RC, Clarke S. Succinimide formation from aspartyl and asparaginyl peptides as a model for the spontaneous degradation of proteins. J Biol Chem 1989;264:6164–6170.
36. Wright HT. Nonenzymatic deamidation of asparaginyl and glutaminyl residues in proteins. Crit Rev Biochem Mol Biol 1991; 26:1–52.
37. Aswad DW. Deamidation and isoaspartate formation in peptides and proteins. CRC Series in Analytical Bio/Technology. Boca Raton, FL: CRC Press; 1995.
38. Robinson NE, Robinson AB. Molecular clocks. Proc Natl Acad Sci USA 2001;98:944–949.
39. Robinson NE, Robinson AB. Molecular clocks: deamidation of asparaginyl and glutaminyl residues in peptides and proteins. Cave Junction, OR: Althouse Press; 2004.
40. Robinson NE, Robinson ZW, Robinson BR, Robinson AL, Robinson JA, Robinson ML, Robinson AB. Structure-dependent nonenzymatic deamidation of glutaminyl and asparaginyl pentapeptides. J Pept Res 2004;63:426–436.
41. Reissner KJ, Aswad DW. Deamidation and isoaspartate formation in proteins: unwanted alterations or surreptitious signals? Cell Mol Life Sci 2003;60:1281–1295.
42. Liu DT. Deamidation: a source of microheterogeneity in pharmaceutical proteins. Trends Biotechnol 1992;10:364–369.
43. Aswad DW, Paranandi MV, Schurter BT. Isoaspartate in peptides and proteins: formation, significance, and analysis. J Pharm Biomed Anal 2000;21:1129–1136.
44. Robinson NE, Robinson AB. Deamidation of human proteins. Proc Natl Acad Sci USA 2001;98:12409–12413.
45. Hoenders HJ, Bloemendal H. Lens proteins and aging. J Gerontol 1983;38:278–286.
46. Takemoto L. Deamidation of Asn-143 of gamma S crystallin from protein aggregates of the human lens. Curr Eye Res 2001; 22:148–153.
47. Hasegawa M, Morishima-Kawashima M, Takio K, Suzuki M, Titani K, Ihara Y. Protein sequence and mass spectrometric analyses of tau in the Alzheimer's disease brain. J Biol Chem 1992;267:17047–17054.
48. Watanabe A, Takio K, Ihara Y. Deamidation and isoaspartate formation in smeared tau in paired helical filaments. Unusual properties of the microtubule-binding domain of tau. J Biol Chem 1999;274:7368–7378.
49. Zhu H, Yang W, Lu W, Zhang J, Shaw GM, Lammer EJ, Finnell RH. A known functional polymorphism (Ile120Val) of the human PCMT1 gene and risk of spina bifida. Mol Genet Metab 2006; 87:66–70.
50. Doyle HA, Gee RJ, Mamula MJ. A failure to repair self-proteins leads to T cell hyperproliferation and autoantibody production. J Immunol 2003;171:2840–2847.
51. Weber DJ, McFadden PN, Caughey B. Measurement of altered aspartyl residues in the scrapie associated form of prion protein. Biochem Biophys Res Commun 1998;246:606–608.
52. Sandmeier E, Hunziker P, Kunz B, Sack R, Christen P. Spontaneous deamidation and isomerization of Asn108 in prion peptide 106–126 and in full-length prion protein. Biochem Biophys Res Commun 1999;261:578–583.
53. Takehara T, Takahashi H. Suppression of Bcl-xL deamidation in human hepatocellular carcinomas. Cancer Res 2003;63:3054–3057.
54. Robinson AB, McKerrow JH, Cary P. Controlled deamidation of peptides and proteins: an experimental hazard and a possible biological timer. Proc Natl Acad Sci USA 1970;66:753–757.
55. Moss CX, Matthews SP, Lamont DJ, Watts C. Asparagine deamidation perturbs antigen presentation on class II major histocompatibility complex molecules. J Biol Chem 2005;280: 18498–18503.

56. Schurter BT, Aswad DW. Analysis of isoaspartate in peptides and proteins without the use of radioisotopes. Anal Biochem 2000;282:227–231.
57. Robinson AB, Rudd CJ. Deamidation of glutaminyl and asparaginyl residues in peptides and proteins. Curr Top Cell Regul 1974;8:247–295.
58. Scotchler JW, Robinson AB. Deamidation of glutaminyl residues: dependence on pH, temperature, and ionic strength. Anal Biochem 1974;59:319–322.
59. Takemoto L, Boyle D. Deamidation of specific glutamine residues from α-A crystallin during aging of the human lens. Biochemistry 1998;37:13681–13685.
60. Robinson NE, Robinson AB. Prediction of protein deamidation rates from primary and three-dimensional structure. Proc Natl Acad Sci USA 2001;98:4367–4372.
61. Robinson NE, Robinson AB, Merrifield RB. Mass spectrometric evaluation of synthetic peptides as primary structure models for peptide and protein deamidation. J Pept Res 2001;57:483–493.
62. Cournoyer JJ, Lin C, O'Connor PB. Detecting deamidation products in proteins by electron capture dissociation. Anal Chem 2006;78:1264–1271.
63. Zomber G, Reuveny S, Garti N, Shafferman A, Elhanany E. Effects of spontaneous deamidation on the cytotoxic activity of the *Bacillus anthracis* protective antigen. J Biol Chem 2005; 280:39897–39906.
64. Robinson NE, Lampi KJ, McIver RT, Williams RH, Muster WC, Kruppa G, Robinson AB. Quantitative measurement of deamidation in lens βB2-crystallin and peptides by direct electrospray injection and fragmentation in a Fourier transform mass spectrometer. Mol Vis 2005;11:1211–1219.
65. Schmid DG, von der Mulbe FD, Fleckenstein B, Weinschenk T, Jung G. Broadband detection electrospray ionization Fourier transform ion cyclotron resonance mass spectrometry to reveal enzymatically and chemically induced deamidation reactions within peptides. Anal Chem 2001;73:6008–6013.
66. Chelius D, Rehder DS, Bondarenko PV. Identification and characterization of deamidation sites in the conserved regions of human immunoglobulin gamma antibodies. Anal Chem 2005;77: 6004–6011.
67. McLafferty FW, Turecek F. Interpretation of mass spectra. Sausalito, CA: University Science Books; 1993.
68. Ivins BE, Welkos SL. Cloning and expression of the *Bacillus anthracis* protective antigen gene in *Bacillus subtilis*. Infect Immun 1986;54:537–542.
69. Worsham PL, Sowers MR. Isolation of an asporogenic (spoOA) protective antigen-producing strain of *Bacillus anthracis*. Can J Microbiol 1999;45:1–8.
70. Farchaus JW, Ribot WJ, Jendrek S, Little SF. Fermentation, purification, and characterization of protective antigen from a recombinant, avirulent strain of *Bacillus anthracis*. Appl Environ Microbiol 1998;64:982–991.
71. Welkos SL, Lowe JR, Eden-McCutchan F, Vodkin M, Leppla SH, Schmidt JJ. Sequence and analysis of the DNA encoding protective antigen of *Bacillus anthracis*. Gene 1988;69:287–300.
72. Powell B, Andrews G, Enama J, Jendrek S, Bolt CR, Worsham P, Pullen J, Ribot W, Hines HB, Smith L, Heath D, Adamovicz J. Design and testing for a non-tagged F1-V fusion protein as vaccine antigen against bubonic and pneumonic plague. Biotechnol Prog 2005;21:1490–1510.
73. Brennan TV, Clarke S. Spontaneous degradation of polypeptides at aspartyl and asparaginyl residues: effects of the solvent dielectric. Protein Sci 1993;2:331–338.
74. Friedlander AM. Macrophages are sensitive to anthrax lethal toxin through an acid-dependent process. J Biol Chem 1986;261: 7123–7126.
75. Hansen MB, Nielsen SE, Berg K. Re-examination and further development of a precise and rapid dye method for measuring cell growth/cell kill. J Immunol Methods 1989;119:203–210.
76. Leppla SH. The anthrax toxin complex. In: Alout JE, Freer JH, editors. Sourcebook of Bacterial Protein Toxins. San Diego, CA: Academic Press; 1991. pp 277–302.
77. Patel K, Borchardt RT. Deamidation of asparaginyl residues in proteins: a potential pathway for chemical degradation of proteins in lyophilized dosage forms. J Parenter Sci Technol 1990; 44:300–301.
78. Capasso S, Mazzarella L, Zagari A. Deamidation via cyclic imide of asparaginyl peptides: dependence on salts, buffers and organic solvents. Pept Res 1991;4:234–238.
79. Cournoyer JJ, Pittman JL, Ivleva VB, Fallows E, Waskell L, Costello CE, O'Connor PB. Deamidation: Differentiation of aspartyl from isoaspartyl products in peptides by electron capture dissociation. Protein Sci 2005;14:452–463.
80. Sarioglu H, Lottspeich F, Walk T, Jung G, Eckerskorn C. Deamidation as a widespread phenomenon in two-dimensional polyacrylamide gel electrophoresis of human blood plasma proteins. Electrophoresis 2000;21:2209–2218.
81. Robinson NE, Robinson AB. Prediction of primary structure deamidation rates of asparaginyl and glutaminyl peptides through steric and catalytic effects. J Pept Res 2004;63:437–448.
82. Petosa C, Collier RJ, Klimpel KR, Leppla SH, Liddington RC. Crystal structure of the anthrax toxin protective antigen. Nature 1997;385:833–838.
83. Lacy DB, Wigelsworth DJ, Melnyk RA, Harrison SC, Collier RJ. Structure of heptameric protective antigen bound to an anthrax toxin receptor: a role for receptor in pH-dependent pore formation. Proc Natl Acad Sci USA 2004;101:13147–13151.
84. Elliott JL, Mogridge J, Collier RJ. A quantitative study of the interactions of *Bacillus anthracis* edema factor and lethal factor with activated protective antigen. Biochemistry 2000;39:6706–6713.
85. Benson EL, Huynh PD, Finkelstein A, Collier RJ. Identification of residues lining the anthrax protective antigen channel. Biochemistry 1998;37:3941–3948.
86. Mogridge J, Cunningham K, Lacy DB, Mourez M, Collier RJ. The lethal and edema factors of anthrax toxin bind only to oligomeric forms of the protective antigen. Proc Natl Acad Sci USA 2002;99:7045–7048.
87. Brossier F, Sirard JC, Guidi-Rontani C, Duflot E, Mock M. Functional analysis of the carboxy-terminal domain of *Bacillus anthracis* protective antigen. Infect Immun 1999;67:964–967.
88. Cunningham K, Lacy DB, Mogridge J, Collier RJ. Mapping the lethal factor and edema factor binding sites on oligomeric anthrax protective antigen. Proc Natl Acad Sci USA 2002;99:7049–7053.